GERMAN-MONGOLIAN
INSTITUTE FOR
RESOURCES AND TECHNOLOGY

The present work was submitted to the
Faculty of Raw Materials and Environmental Engineering

VALIDATION OF AN ALTERNATIVE ANALYZATION METHOD FOR MANUAL SORTING TO ANALYZE LARGER PARTICLE SIZE FRACTIONS FROM RECYCLING LITHIUM-ION BATTERIES (LIBs)

Bachelor Thesis

By

Sainzaya Odbayar

Study program: Raw Materials and Process Engineering
Student ID: B2200475

Supervisor 1 / Examiner 1	Prof. rer. nat. Purev-Ochir Togtokhbaatar
Supervisor 2 / Examiner 2	Prof. Dr.-Ing. Urs A. Peuker

Ulaanbaatar/Nalaikh, 01/05/2026

GERMAN-MONGOLIAN
INSTITUTE FOR
RESOURCES AND TECHNOLOGY

The present work was submitted to the
Faculty of Raw Materials and Environmental Engineering

VALIDATION OF AN ALTERNATIVE ANALYZATION METHOD FOR MANUAL SORTING TO ANALYZE LARGER PARTICLE SIZE FRACTIONS FROM RECYCLING LITHIUM-ION BATTERIES (LIBs)

Bachelor Thesis

By

Sainzaya Odbayar

Study program: Raw Materials and Process Engineering
Student ID: B2200475

Supervisor 1 / Examiner 1	Prof. rer. nat. Purev-Ochir Togtokhbaatar
Supervisor 2 / Examiner 2	Prof. Dr.-Ing. Urs A. Peuker

Ulaanbaatar/Nalaikh, 01/05/2026

GERMAN-MONGOLIAN
INSTITUTE FOR
RESOURCES AND TECHNOLOGY

Statutory Declaration

Odbayar, Sainzaya	B2200475
Last Name, First Name	Student ID Number

I hereby affirm in lieu of an oath that I provided the submitted bachelor thesis

VALIDATION OF AN ALTERNATIVE ANALYZATION METHOD FOR MANUAL SORTING TO ANALYZE LARGER PARTICLE SIZE FRACTIONS FROM RECYCLING LITHIUM-ION BATTERIES (LIBs)

I did not use any sources other than those stated. In case that the work is additionally submitted on a data medium, I declare that the written and the electronic form are completely identical. The work was not submitted in the same or similar form to any examination authority.

Place, Date	Signature

Abstract

This thesis investigates the use of ShredCat shredding combined with inductively coupled plasma optical emission spectrometry (ICP-OES) analysis as an alternative to manual sorting for the compositional characterization of larger particle size fractions from shredded lithium-ion batteries (LIBs). The results demonstrate that the method achieves low mass loss and produces consistent, reproducible measurements across different battery types.

The study used model material comprising mixtures of metal foils and black mass (BM) at three different particle size fractions, as well as real foil fractions obtained from various battery types. All samples were processed through two-step crushing by ShredCat, divided using a rotary splitter, and analyzed by ICP-OES. Sieve analysis was additionally carried out to characterize the particle size distribution of the real foil fractions prior to processing.

Mass loss during ShredCat processing was lower for real foil fractions than for model materials, which is attributed to the active coating material being closely adhered to the foil surfaces rather than present as free powder. Among the particle size fractions tested, the above 0.25 mm fraction showed the closest agreement with expected compositions following mass loss correction. Comparison with manual sorting results indicated that manual sorting tends to under-recover metals and active material relative to the ShredCat method, particularly in air-classified samples. Elemental compositions also varied considerably between different battery types, highlighting the need for cell-type-specific reference values.

Efficient and accurate characterization of coarse fractions is an important requirement in LIB recycling process development. The ShredCat method addresses the key limitations of manual sorting, namely its low throughput, susceptibility to human error, and restriction to small sample masses, and offers a more scalable approach to support the optimization of recycling processes in line with EU material recovery targets.

GERMAN-MONGOLIAN
INSTITUTE FOR
RESOURCES AND TECHNOLOGY

Acknowledgements

First and foremost, I would like to express my sincere gratitude to the German-Mongolian Institute of Technology (GMIT) and the Technische Universität Bergakademie Freiberg (TUBAF) for providing the opportunity to participate in an exchange program that allowed me to conduct the experimental work for this thesis in the laboratories of TUBAF's Institute for Mechanical Process Engineering and Mineral Processing. The experience was deeply rewarding, both academically and personally.

I would also like to sincerely thank my supervisors, Prof. rer. nat. Purev-Ochir Togtokhbaatar and Prof. Dr.-Ing. Urs A. Peuker, for their guidance, expertise, and support throughout this work. Their knowledge and encouragement were invaluable in shaping this thesis.

I am likewise grateful to Mr. Simon F. Bendl for his substantial guidance and support throughout the course of this research, and to Mrs. Yvonne Volkmar for conducting all ICP-OES analyses, which formed an essential part of the experimental work.

My thanks also go to my friends and fellow students, particularly those in the Raw Materials and Process Engineering (RPME) program, for their companionship and encouragement throughout this journey.

Finally, I am deeply grateful to my family for their unwavering support and encouragement throughout my studies.

Table of Contents

List of figures V

List of tables VI

List of abbreviations and symbols VII

1. Introduction 1

2. Literature review 3

3. Materials and methods 7

3.1. Materials 7

3.1.1. Sample description 7

3.1.2. Equipment 13

3.2. Methodology 16

3.2.1. Model material analysis 17

3.2.2. Manual sorting vs ShredCat 17

3.2.3. Real foil fractions with different cell types 17

4. Results 18

4.1. Model material analysis 18

4.2. Manual sorting vs ShredCat 26

4.3. Real foil fractions with different cell types 26

5. Discussion 29

6. Conclusion 32

7. Future Work 34

References 35

Appendix A: Non-disclosure agreement 38

Appendix B: User manual 43

Appendix C: Raw data 44

List of figures

Figure 1. Structure of LIB cell and its functional unit. Source: Kaas, Alexandra, 2025 ... 3
Figure 2. Schematic of the TUBAF recycling process. Source: Kaas, Alexandra, 2025 . 5
Figure 3. Close-up comparison of Cu (a) and Al (b) foil surfaces ... 8
Figure 4. Model material mixture (a) unmixed and (b) mixed ... 8
Figure 5. Physical appearance of the real foil fractions ... 10
Figure 6. Cumulative particle size distribution (PSD) curve of pre-ShredCat real foil fraction ... 12
Figure 7. (a) IDEAL ShredCat 8200. Source: IDEAL, n.d. (ideal.de) (b) close-up view of modification area ... 13
Figure 8. Dickie & Stockler 30 L 12-way Divider: Front and Side Views ... 14
Figure 9. (a) Haver & Boecker EML Digital Plus sieve shaker with stacked sieve tower for particle size separation. (b) Digital control panel showing settings and operation parameters. ... 15
Figure 10. Main experiment flow chart (a) model material preparation (b) crushing process (c) DS rotary splitter. Source: rseprojects.co.za (d) ICP-OES equipment set-up. Source: eal.ucmerced.edu ... 16
Figure 11. Mass loss comparison across foil fractions ... 19
Figure 12. Comparative mass loss in ShredCat_1 and ShredCat_2 ... 19
Figure 13. ShredCat_1: pre-cleaning and post-cleaning state ... 20
Figure 14. Comparison of relative wt.-% difference for each element between the calculated model material composition and the ShredCat analysis results ... 22
Figure 15. Comparison of relative wt.-% difference for each element between the measured ShredCat analysis results and the refined composition after first estimation correction ... 24
Figure 16. Comparison of relative wt.-% difference for each element between the measured ShredCat analysis results and the refined composition after second estimation correction ... 25
Figure 17. Cumulative particle size distribution (PSD) curve of after-ShredCat real foil fraction ... 28

List of tables

Table 1. Model material's each components' element content 8
Table 2. Mass of each component by three foil fractions 9
Table 3. Element content of three foil fractions 9
Table 4. Particle size distribution (PSD) analysis of pre-ShredCat real foil fraction 12
Table 5. Mass loss comparison of three foil fraction sizes 18
Table 6. Relative wt.-% difference between ShredCat method's ICP-OES elemental composition and model material composition in Table 3 21
Table 7. Corrected wt.-% composition of elements following first estimation 23
Table 8. Corrected wt.-% composition of elements following second estimation 24
Table 9. Relative wt.-% difference: manual sorting vs ShredCat analysis 26
Table 10. Elemental wt.-% composition by cell type 27
Table 11. Particle size distribution (PSD) analysis of after-ShredCat real foil fraction 27
Table 12. Raw data for model material 44
Table 13. Raw data for manual sorting vs ShredCat analysis 44
Table 14. Raw data for real foil fraction with different cell types 44

List of abbreviations and symbols

Abbreviations

AC	Air classification
Al	Aluminum
Al	Aluminum foil
Al_2O_3	Aluminum oxide
BM	Black mass
BM_1	Black mass after first classification
BM_2	Black mass after second classification
CAM	Cathode active material
CMC	Carboxymethyl cellulose
Co	Cobalt
Cu	Copper
Cu	Copper foil
DEC	Diethyl carbonate
DMC	Dimethyl carbonate
EC	Ethylene carbonate
EMC	Ethyl methyl carbonate
EU	European Union
EVs	Electric vehicles
EoL	End-of-life
Fe	Iron
HCl	Hydrochloric acid
HNO_3	Nitric acid
ICP-OES	Inductively Coupled Plasma Optical Emission Spectrometer
Li	Lithium
LIB	Lithium-ion battery
LIBs	Lithium-ion batteries
$LiPF_6$	Lithium hexafluorophosphate
Mn	Manganese
NCA	Lithium nickel cobalt aluminum oxide
Ni	Nickel
NMC	Lithium nickel manganese cobalt oxide
P	Phosphorus
PC	Propylene carbonate

PE	Polyethylene
PP	Polypropylene
PSD	Particle size distribution
PTC	Discharge method with positive temperature coefficient
PVDF	Polyvinylidene fluoride
SBR	Styrene-butadiene rubber
SEI	Solid electrolyte interface
SEM	Scanning electron microscope
SoC	State of charge
TUBAF	Technische Universität Bergakademie Freiberg
wt.-%	Weight percentage
ZZS	Zig-zag air classifier

Symbols

M_{Co}	Molar mass of cobalt
M_F	Molar mass of fluorine
M_{Li}	Molar mass of lithium
M_{Mn}	Molar mass of manganese
M_{Ni}	Molar mass of nickel
M_O	Molar mass of oxygen
M_P	Molar mass of phosphorus
$c_{Al,CAM}$	wt.-% of Al in CAM
c_{CAM}	wt.-% of CAM
$c_{Co,CAM}$	wt.-% of Co in CAM
c_{LiPF_6}	wt.-% of Li in $LiPF_6$
$c_{Mn,CAM}$	wt.-% of Mn in CAM
$c_{Ni,CAM}$	wt.-% of Ni in CAM
$c_{P,LiPF_6}$	wt.-% of P in $LiPF_6$
m_0	Mass before crushing
m	Mass after crushing
Δm	Mass loss in g
m_b	Batch mass

1. Introduction

The accelerating global transition towards electromobility and renewable energy storage has placed lithium-ion batteries (LIBs) at the center of modern energy infrastructure. As demand for LIBs continues to grow, driven by the rapid expansion of electric vehicles (EVs) and stationary energy storage systems, so does the urgency of addressing the environmental and resource challenges posed by their end-of-life (EoL) management. LIBs contain a range of valuable and critical raw materials, including lithium (Li), cobalt (Co), nickel (Ni), and manganese (Mn), whose extraction is both resource-intensive and environmentally damaging. At the same time, improper disposal of spent LIBs carries significant risks due to the toxicity of their chemical components and the potential for thermal runaway. Establishing efficient and scalable recycling processes is therefore an environmental imperative and a strategic necessity for securing the supply of critical materials within a circular economy. In recent years, both legislative frameworks and industrial investment have reflected this urgency, with the EU Battery Regulation and similar policies worldwide pushing for higher recycling efficiencies and material recovery rates.

A central challenge in LIB recycling research lies in the characterization of shredded battery material, particularly in analyzing the composition of larger particle size fractions produced during mechanical pre-treatment. The standard approach to this analysis is manual sorting, in which particles are physically separated and identified by hand. While manual sorting provides reliable compositional data, it is inherently limited in throughput: the labor-intensive nature of the process restricts analyses to relatively small sample masses, which may not adequately represent the heterogeneity of industrial-scale material streams. Furthermore, the method is difficult to standardize and scale, creating a bottleneck in both research and quality control within recycling operations. To date, no well-established alternative exists for the analysis of larger particle fractions, leaving a significant methodological gap in the field and motivating the search for a more scalable analytical approach.

This thesis addresses that gap by investigating ShredCat as a potential alternative to manual sorting for the compositional analysis of coarse particle fractions from shredded LIBs. The central objective is to validate ShredCat as a reliable analytical method capable of replacing or complementing manual sorting. The validation process is structured in several steps. First, the method is applied to model materials, which are well-defined reference samples of known composition, in order to assess its accuracy and repeatability under controlled conditions. Second, ShredCat is applied to real foil fractions derived from recycled LIBs, and the results are compared against compositional

data obtained through manual sorting in previous studies, thereby benchmarking the new method against the established standard. Finally, recognizing that one of the key limitations of manual sorting is the restriction to small sample masses, the thesis extends the analysis of real foil fractions to significantly larger sample quantities than those typically feasible with manual handling. This final step is critical for assessing whether ShredCat can deliver representative and consistent results at a scale relevant to industrial applications.

2. Literature review

LIBs are rechargeable electrochemical energy storage devices used across a wide range of applications, from small portable electronics to grid-scale power storage stations, owing to their high efficiency, long cycle life, and high power and energy densities. [1] One significant driver of growing LIB demand is the rapid expansion of EVs. [2] As global efforts to reduce greenhouse gas emissions gain momentum, interest in EVs has increased, given their potential to eliminate the carbon emissions associated with road transport. [3] However, this shift also generates a growing volume of end-of-life LIBs, which presents ongoing challenges for engineers seeking less expensive and more environmentally friendly recycling solutions, as well as for legislators working to regulate current practices and plan for future volumes. [4] In parallel, European policy has tightened recovery requirements; Regulation (EU) 2023/1542 sets staged minimum recovery rates for Co, Ni, Cu, and Li, pushing industry away from purely pyrometallurgical routes towards process chains that combine mechanical pre-treatment with hydrometallurgical refining and, in the longer term, direct recycling of cathode active materials. [5] [6]

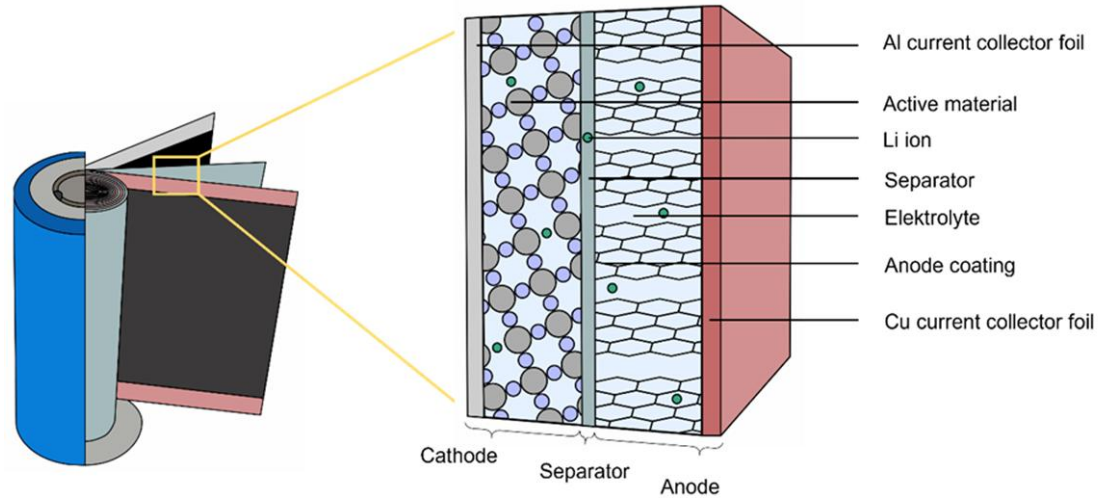


Figure 1. Structure of LIB cell and its functional unit. Source: Kaas, Alexandra, 2025

The most common LIB cell structure consists of a functional unit comprising an anode and a cathode coated on metallic current collectors, a separator, an electrolyte, and a casing (Fig. 1). [5] [1] The anode is a copper current collector foil coated predominantly with graphite, whose widespread use reflects its stable thermal and mechanical behavior, good electrical conductivity, and low toxicity. [7] During formation, the anode material must facilitate the development of a solid electrolyte interface (SEI), a 10 to 50 nm passivation layer that suppresses further electrolyte decomposition and strongly influences cycle stability and cell lifetime. [1] To ensure dense packing of coating

particles and good adhesion to the copper foil, organic binders are used, typically polyvinylidene fluoride (PVDF) or water-soluble blends of carboxymethyl cellulose (CMC) and styrene-butadiene rubber (SBR). [5] [7] Overall, the anode accounts for roughly 27 to 29 wt.-% of the total cell mass.

The cathode consists of an aluminum current collector foil coated with cathode active material (CAM). In contrast to the anode, CAM chemistries are diverse; the current state of the art comprises layered lithium metal oxides such as lithium nickel manganese cobalt oxide (NMC) and lithium nickel cobalt aluminum oxide (NCA), in which Ni, Mn, Co, and Al appear in varying stoichiometric ratios. This cathode composite typically contributes around 28 to 31 wt.-% of the total cell mass.

The separator is a safety-critical, semipermeable polymer membrane that prevents electronic short circuits between the anode and cathode while allowing Li-ions to migrate through its pores, thereby enabling charge transfer. It is generally made from polypropylene (PP), polyethylene (PE), or a PP-PE-PP trilayer, and represents approximately 4 to 5 wt.-% of the cell mass.

The electrolyte is a mixture of organic carbonate solvents and a dissolved lithium salt that provides ionic conductivity between the electrodes, enabling Li-ion transport and the conversion of chemical energy into electrical energy. It must combine low viscosity, a sufficient dielectric constant, and electrochemical stability. In practice, mixtures of linear carbonates, including dimethyl carbonate (DMC), ethyl methyl carbonate (EMC), and diethyl carbonate (DEC), and cyclic carbonates, including ethylene carbonate (EC) and propylene carbonate (PC), with lithium hexafluorophosphate ($LiPF_6$) as the conductive salt are predominantly used.

The casing encloses and protects the functional unit of the cell, preventing moisture ingress and electrolyte loss. Moisture exclusion is essential to avoid $LiPF_6$ hydrolysis and the associated formation of hydrogen fluoride, while the need to retain volatile electrolyte components rules out purely plastic housings. Consequently, casings are made from aluminum, steel, or an aluminum-polymer laminate in the case of pouch cells. [7]

Three principal recycling routes are discussed in the literature: pyrometallurgy, hydrometallurgy, and direct recycling, each typically preceded by mechanical pre-treatment. [4] High-temperature pyrometallurgical smelting (approximately 1400 °C) recovers Ni, Co, and Cu into a metallic phase, while Li and Al report to the slag, which can be leached but is not routinely exploited in current industrial practice. [2] Hydrometallurgical flowsheets leach metals from black mass using mineral or organic acids, followed by selective precipitation, solvent extraction, or electrochemical separation. These processes can re-synthesize cathode active materials, but require a reasonably pure black mass input with controlled levels of Al, Cu, Fe, and electrolyte

residues. Direct recycling aims to preserve the crystal structure of cathode oxides through gentle liberation and relithiation, which is particularly attractive for NMC and LFP chemistries. However, it remains largely at laboratory or pilot scale and relies on manual or semi-manual feed preparation.

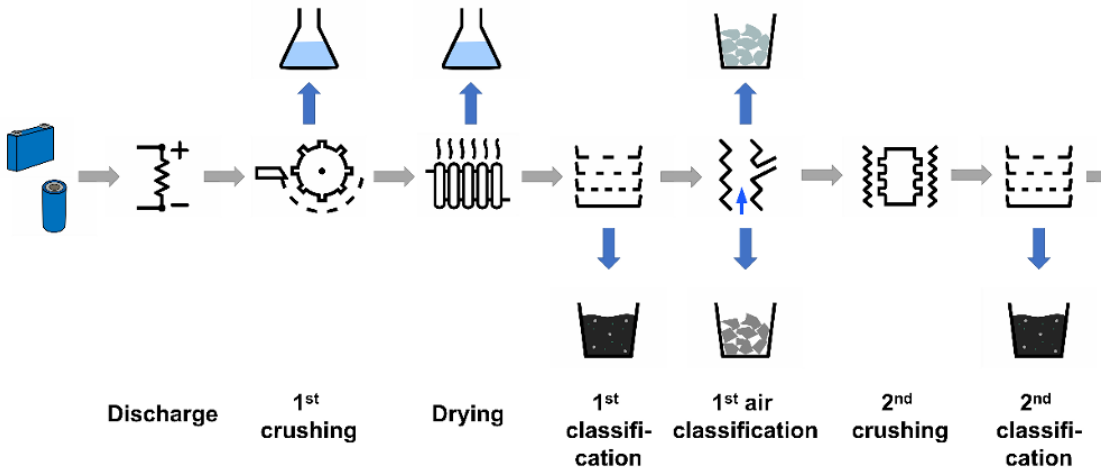


Figure 2. Schematic of the TUBAF recycling process. Source: Kaas, Alexandra, 2025

Prior to this thesis, the TUBAF mechanical recycling process had been studied as a two-stage dry process that converts whole cells into black mass and metal concentrates through discharge, comminution, drying, sieving, and zig-zag air classification (ZZS).

Figure 2 summarizes the experimental flowsheet and sampling strategy, showing the discharge of individual cells, two-stage crushing with intermediate drying, production of BM_1 and BM_2 by sieving at 1 mm and 500 µm, and both ZZS steps that generate separator, casing, cathode, and anode fractions for subsequent mass balance and IC OES analysis.

Cells are first over-discharged below 0% state of charge (SoC) using a PTC resistance to avoid thermal runaway during crushing. Deeper over-discharge into pole reversal is deliberately avoided in the reference process, as it causes copper dissolution and redeposition on the cathode and separator, which subsequently appears as elevated Cu contamination in the black mass and coated separator compounds. Discharged cells are then crushed in a slow twin-shaft pre-crusher and a fast single-shaft rotary shear with a 20 mm grid, dried at ambient temperature to remove volatile electrolyte, and sieved at 1 mm to produce the first black mass (BM_1). The coarse residue passes through a ZZS to separate a light separator fraction, a heavy casing fraction, and an intermediate electrode fraction. This electrode fraction is decoated in a high-speed impact mill at moderate specific stress energies to avoid excessive foil attrition, followed by a second

sieving at 500 µm to obtain the second black mass (BM_2). A final ZZS step at intermediate air velocity then splits the material into Al-rich cathode and Cu-rich anode concentrates.

Overall, BM_1 and BM_2 together recover roughly 60 to 65 wt.-% of the cell mass and can meet EU recovery targets for Li, Ni, and Co under optimized conditions. However, Cu and Al impurities remain governed by discharge history, foil fragmentation, and coated separator formation, and no mechanical route alone has yet demonstrated 95% Cu recovery from realistic mixed automotive streams. [5] [7]

Most current work on mechanical pre-treatment and material recovery in LIB recycling focuses on the fine black mass fraction obtained after air classification and sieving, typically defined as the below 0.25 to 0.5 mm size class. In contrast, the coarser fractions remain poorly investigated and are studied mainly through manual sorting rather than structured, quantitative process analysis. These larger particles consist predominantly of current collector foils, casing metals, and separator foils. Effective comminution of this material not only increases the surface area available for subsequent chemical or metallurgical processing, but can also liberate active material that remains trapped in partially coated or composite particles.

Manual handling of these coarse fractions is a poor basis for process design. It is extremely time-consuming, limits the feasible sample mass, is prone to human error, and cannot detect differences in internal coating structure between cell types that are not visible from the outside. As a result, the composition and elemental distribution of the coarse fractions remain only roughly known, and their contribution to overall recovery and loss pathways has not yet been well quantified.

3. Materials and methods

This thesis aims to validate an alternative method to manual sorting for analyzing the larger particle size fractions of shredded LIBs. The alternative method under investigation makes use of a paper shredder called ShredCat, which was selected based on the characteristics of the feed material.

Manual sorting has previously been used to analyze the larger particle size fractions, but it is time-consuming, labor-intensive, and prone to human error. The primary limitation of manual sorting is that, due to its reliance on human handling, the precise proportion and composition of the foil fraction cannot be determined with certainty.

3.1. Materials

3.1.1. Sample description

The samples used in the experiments consisted of model material and real foil fractions of shredded LIBs. Model material was used initially to test the method, as it is reproducible and has a controlled, known composition, making it a more reliable starting point than working directly with real foil fractions. The model material was designed based on the results of a previous study and comprised aluminum foil (Al), copper foil (Cu), separator foil, and black mass (BM).

The aluminum and copper foils were pure metals, free of contaminants. The Al foil occurred as thin, flake-like fragments, while the Cu foil consisted of smaller, irregular fragments. The separator was similarly clean but was cut to achieve a particle size comparable to that of the real foil fraction. The black mass, by contrast, consisted of very fine particles.

ICP-OES analysis of the BM yielded a comprehensive list of detected elements: Al, Cu, Co, Fe, Ni, Mn, Li, and P. The concentration of cathode active material (CAM) was calculated from the measured concentrations of Co, Mn, and Ni according to Eq. (1), and the concentration of $LiPF_6$ was calculated from the P concentration according to Eq. (2).

$$c_{CAM} = \left(c_{Co,CAM} + c_{Mn,CAM} + c_{Ni,CAM}\right) + \left(\frac{c_{Co,CAM}}{M_{Co}} + \frac{c_{Mn,CAM}}{M_{Mn}} + \frac{c_{Ni,CAM}}{M_{Ni}}\right) \times \left(M_{Li} + 2 \cdot M_O\right) \quad (1)$$

$$c_{LiPF_6} = \frac{c_{P,LiPF_6}}{M_P} \times \left(M_{Li} + M_P + 6 \cdot M_F\right) \quad (2)$$

$$c_{Rest} = 100\% - c_{Al} - c_{Cu} - c_{Fe} - c_{CAM} - c_{LiPF_6} \quad (3)$$

Raw data for Eqs. (1) to (3) are provided in Appendix C.

The concentrations of Fe and $LiPF_6$ were too low to be significant and were therefore excluded from further calculations. The remaining fraction, after accounting for Al, Cu, Fe, CAM, and $LiPF_6$, was designated as Rest according to Eq. (3). The resulting initial elemental weight percentages of the model material components are presented in Table 1.

Table 1. Model material's each components' element content

Element / Component	Al	Cu	CAM	Rest
	wt.-%	wt.-%	wt.-%	wt.-%
Aluminum foil	100	-	-	-
Copper foil	-	100	-	-
Separator foil	-	-	-	100
Black mass	0.35	0.87	58.20	38.69

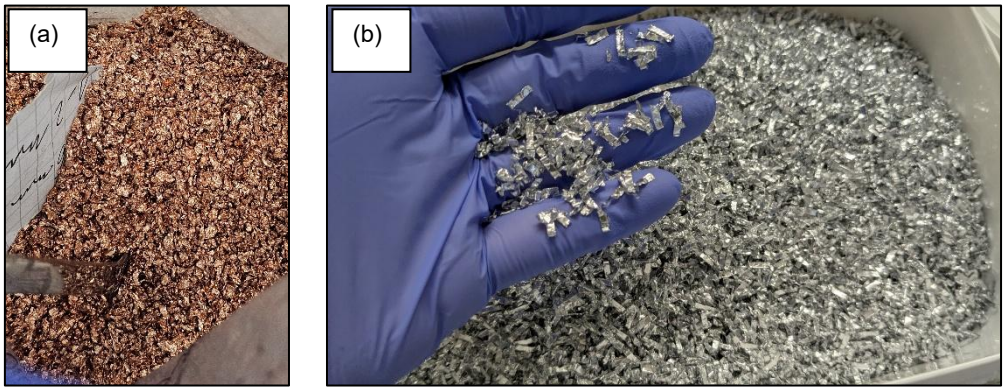


Figure 3. Close-up comparison of Cu (a) and Al (b) foil surfaces

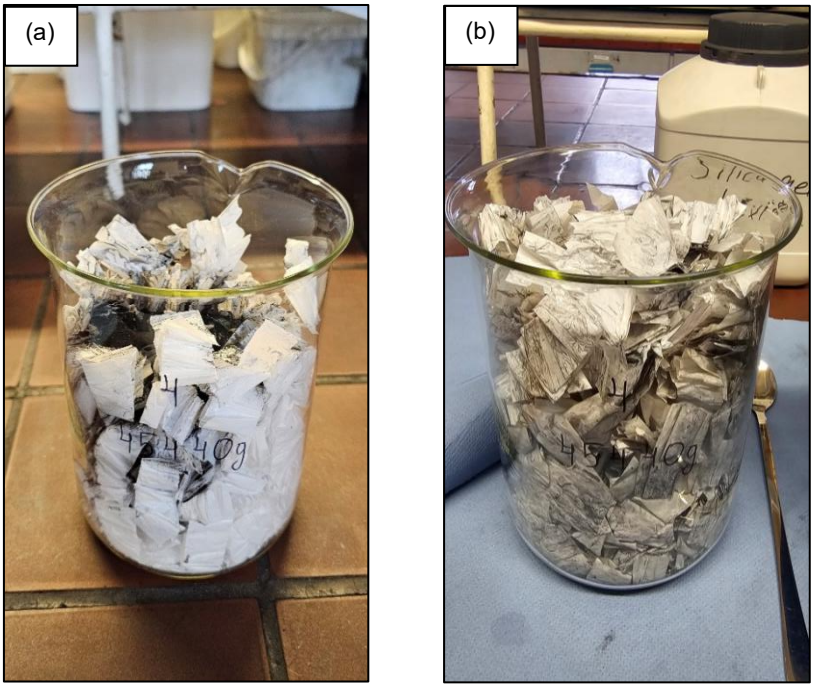


Figure 4. Model material mixture (a) unmixed and (b) mixed

The larger particle size fractions studied in this thesis have a broad particle size distribution, ranging from 0.25 mm to 20 mm. To determine whether pre-sieving into size classes improves the ShredCat method, or whether processing the entire fraction directly is more effective, the model material was classified into three particle size fractions: above 4 mm, above 2 mm, and above 0.25 mm. All components were weighed and mixed in a beaker prior to further processing, with the compositions of each fraction presented in Table 2.

Table 2. Mass of each component by three foil fractions

	> 4 mm	**> 2 mm**	**> 0.25 mm**
Al foil	1.25 g	4 g	20 g
Cu foil	1.25 g	4 g	20 g
Separator	15 g	16 g	10 g
Black mass (BM)	7.5 g	16 g	50 g
Batch mass, m_b	25 g	40 g	100 g

The elemental content of the three foil fractions was calculated using Eq. (4) and the results are shown in Table 3.

$$c_{element}(\%) = \frac{1}{m_b}\sum_{j=1}^{1} m_j \cdot c_{element,j} \quad (4)$$

An example calculation of element content in > 0.25 mm fraction:

$$c_{Al}(\%) = \frac{1}{100\ g} \cdot (20\ g \cdot 100\% + 20\ g \cdot 0\% + 10\ g \cdot 0\% + 50\ g \cdot 0.35\%) = 20.17\ wt.-\%$$

$$c_{Cu}(\%) = \frac{1}{100\ g} \cdot (20\ g \cdot 0\% + 20\ g \cdot 100\% + 10\ g \cdot 0\% + 50\ g \cdot 0.87\%) = 20.44\ wt.-\%$$

$$c_{CAM}(\%) = \frac{1}{100\ g} \cdot (20\ g \cdot 0\% + 20\ g \cdot 0\% + 10\ g \cdot 0\% + 50\ g \cdot 58.20\%) = 29.09\ wt.-\%$$

$$c_{Rest}(\%) = \frac{1}{100\ g} \cdot (20\ g \cdot 0\% + 20\ g \cdot 0\% + 10\ g \cdot 100 + 50\ g \cdot 38.69\%) = 29.36\ wt.-\%$$

Table 3. Element content of three foil fractions

	Al	**Cu**	**CAM**	**Rest**
	wt.-%	**wt.-%**	**wt.-%**	**wt.-%**
> 4 mm	5.10	5.26	17.46	71.61
> 2 mm	10.16	10.34	23.26	55.48
> 0.25 mm	20.17	20.44	29.09	29.36

The real foil fraction of the larger particle size, shown in Fig. 5, consisted predominantly of separator foils with a fibrous, irregular morphology and blackish residual active material adhered to their surfaces. Using real foil fractions, a total of ten experiments were conducted with ShredCat. Nine experiments focused on ShredCat processing analysis, while one was dedicated solely to particle size distribution (PSD) analysis prior to ShredCat processing.



Figure 5. Physical appearance of the real foil fractions

Of the nine processing experiments, six used real foil fractions generated from manual sorting experiments, where the available sample mass was low due to the inherently small sample sizes associated with manual sorting. Four of these six fractions were generated from air classification products, one of which came from a different cell type whose separator foil was coated with aluminum oxide (Al_2O_3). The remaining two of the six fractions were generated from sieving. The last three of the nine experiments used real foil fractions from different cell types: one pouch cell with a particle size fraction above 0.25 mm, and two prismatic cells with particle size fractions above 0.5 mm and above 0.25 mm respectively.

One additional above 0.5 mm real foil fraction sample was subjected to PSD analysis only, prior to ShredCat processing. Sieve analysis was conducted according to Table 4, with the foil fraction retained on each sieve deck weighed to establish cumulative distributions. From the results, mass fraction, cumulative distribution, and distribution density were calculated according to Eqs. (5) to (8).

The PSD curve (Fig. 6) shows that the foil fraction is strongly dominated by fine particles, with approximately 54 wt.-% falling between 0.5 and 2 mm and around 81 wt.-% passing 8 mm. Only a small fraction lies in the coarse range. The distribution density values confirm the dominance of the finer size classes, with the highest densities recorded in the 0.5 to 1 mm and 1 to 2 mm classes (approximately 43 and 33 %/mm respectively) and moderate densities of roughly 2 to 6 %/mm in the 2 to 8 mm range. In

all size classes above 8 mm, density values drop to very low levels, falling to near zero above 16 mm.

Mass fraction:

$$\mu_{3,i} = \frac{m_{3,i}}{m_t} \cdot 100\% \quad (5)$$

Cumulative passing distribution:

$$Q_{3,i}(x) = \sum_{a=1}^{i} \mu_{3,a} \quad (6)$$

Cumulative residue distribution:

$$R_{3,i}(x) = 100\% - Q_{3,i}(x) \quad (7)$$

Distribution density:

$$q_{3,i}(x) = \frac{\mu_{3,i}}{\Delta x_i} \quad (8)$$

An example calculation at 2 mm:

$$\mu_{3,i} = \frac{61.4\ g}{535.8\ g} \cdot 100\% = 11.46\%$$

$$Q_{3,i}(x) = \sum_{a=1}^{i} \mu_{3,a} = 11.46 + 32.74 + 21.67 = 65.86\%$$

$$R_{3,i}(x) = 100\% - Q_{3,i}(x) = 100\% - 65.86\% = 34.14\%$$

$$q_{3,i}(x) = \frac{\mu_{3,i}}{\Delta x_i} = \frac{11.46\%}{2\ mm} = 5.73\ \frac{\%}{mm}$$

Table 4. Particle size distribution (PSD) analysis of pre-ShredCat real foil fraction

Class		**Mass**	**Mass fraction**	**Cumulative distr.**		**Class width**	**Distr. density**
$x\ [mm]$		$m_{3,i}\ [g]$	$\mu_{3,i}\ [\%]$	$Q_{3,i}(x)\ [\%]$	$R_{3,i}(x)\ [\%]$	$\Delta x_i\ [mm]$	$q_{3,i}(x)\ \left[\frac{\%}{mm}\right]$
25	-	0	-	-	-	-	-
20	25	0.4	0.07	100	0	5	0.015
16	20	5	0.93	99.93	0.07	4	0.233
12.5	16	18.6	3.47	98.99	1.01	3.5	0.992
10	12.5	55.1	10.28	95.52	4.48	2.5	4.113
8	10	22.7	4.24	85.24	14.76	2	2.118
4	8	81.1	15.14	81.00	19.00	4	3.784
2	4	61.4	11.46	65.86	34.14	2	5.730
1	2	175.4	32.74	54.40	45.60	1	32.736
0.5	1	116.1	21.67	21.67	78.33	0.5	43.337
0	0.5	0	0	0	100	0.5	0
Total, m_t		535.8	100	0	100	-	-

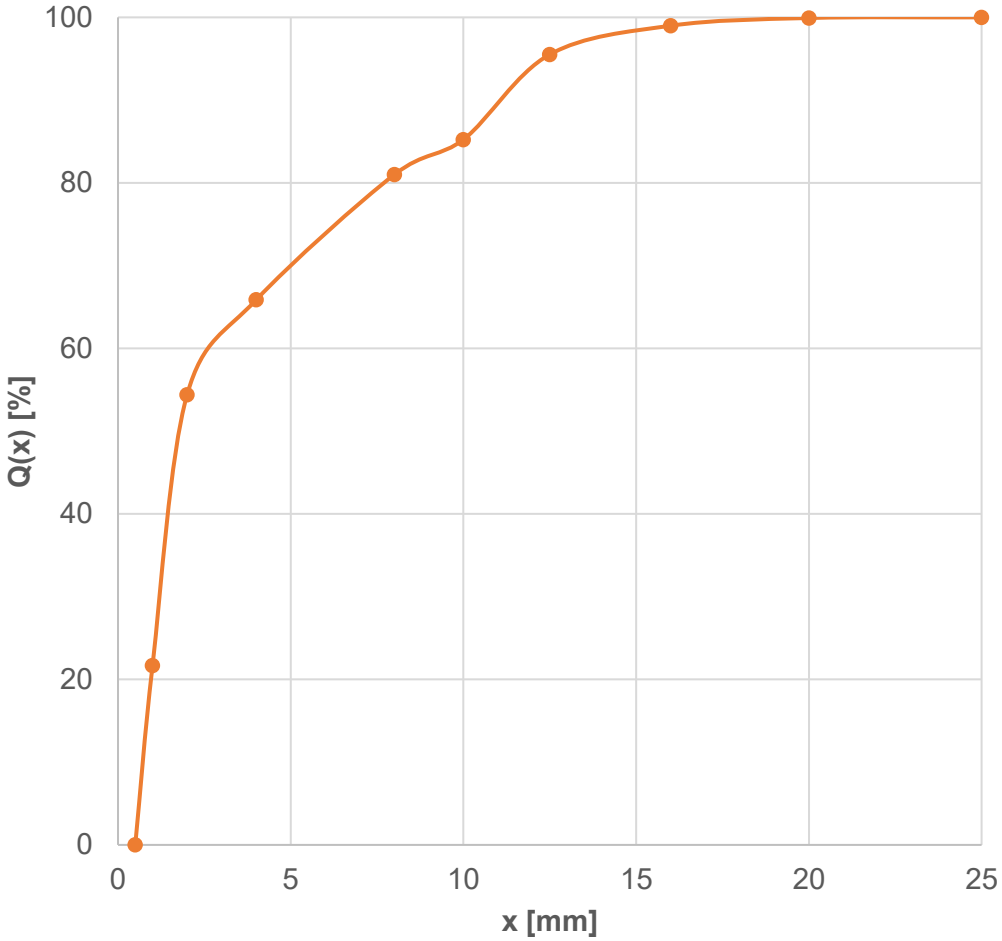


Figure 6. Cumulative particle size distribution (PSD) curve of pre-ShredCat real foil fraction

3.1.2. Equipment

ShredCat

The foil fractions exhibit ductile, fibrous behavior rather than brittle fracture. [8] Comminution machines that combine shearing, cutting, and tearing stresses at low speeds (circumferential velocity of 5 m/s or below) have been shown to be effective in processing scrap metal and mixed debris that does not exhibit brittle behavior. [9] The two-step crushing was therefore performed using an IDEAL ShredCat 8200 cross-cut shredder (IDEAL Krug & Priester GmbH & Co. KG, Germany). The shredder has a multi-function switch for forward, stop, and reverse operation. The automatic start/stop function controlled by the light barrier was disabled to allow continuous, controlled feeding during experiments.

Initially, the first shredder (ShredCat_1) was used until it broke down during the experiments. A second shredder (ShredCat_2) was then introduced, to which an additional internal design modification was made to reduce black mass fine dust loss. A 3D-printed connector part was fitted between the cross-cutter and the feed outlet opening, where BM loss had been identified. ShredCat_2 was operated in 10-minute intervals with 10-minute rest periods between runs.

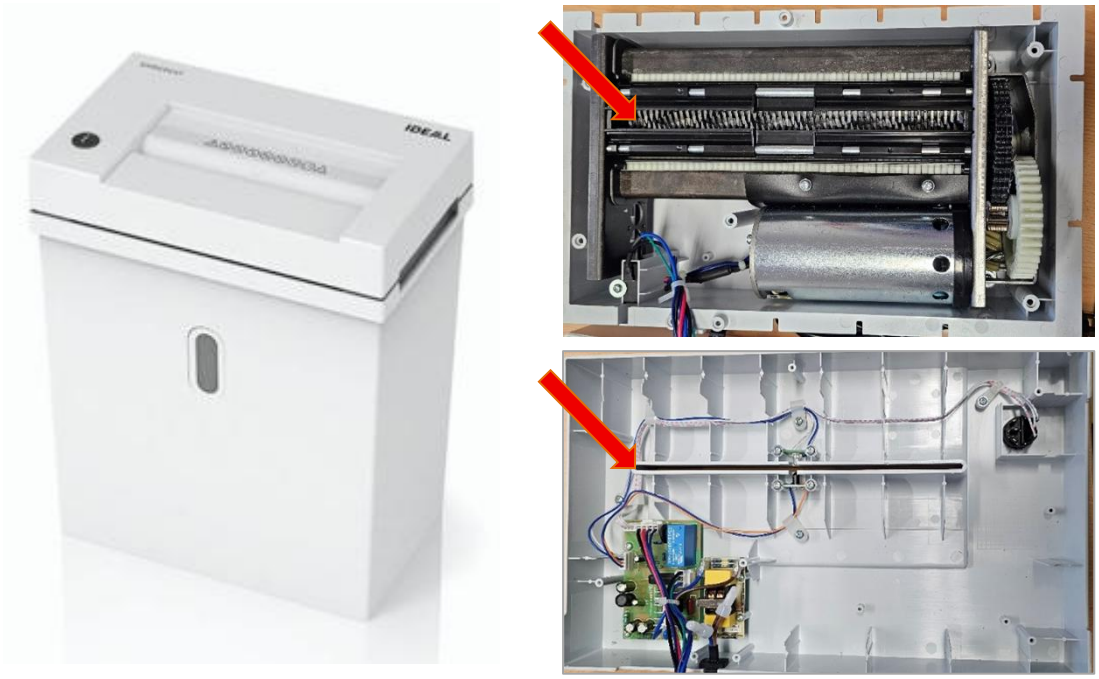


Figure 7. (a) IDEAL ShredCat 8200. Source: IDEAL, n.d. (ideal.de) (b) close-up view of modification area

DS rotary splitter

Following the two-step crushing, samples were divided using a DS rotary splitter (Dickie & Stockler, 30 L, 12-way divider) to obtain representative sub-samples for ICP-OES analysis. Rotary splitting divides the bulk material into equal portions by continuously rotating the sample stream across all 12 sample containers, thereby reducing sub-sampling bias. A 30 L splitter was used despite the sample mass being below 100 g in most cases, because the discharge diameter of the conical feed must be three to four times larger than the largest particle in the feed. Uniform, non-segregating feed flow was critical during the experiments, as the samples contained particles ranging from fine BM dust to separator and metal foils, which differ considerably in size and density and could cause blockages or uneven distribution across the sample containers. Of the 12 divided sub-samples, 8 were selected for ICP-OES analysis, and the reported elemental concentrations represent the average of those 8 sub-samples.

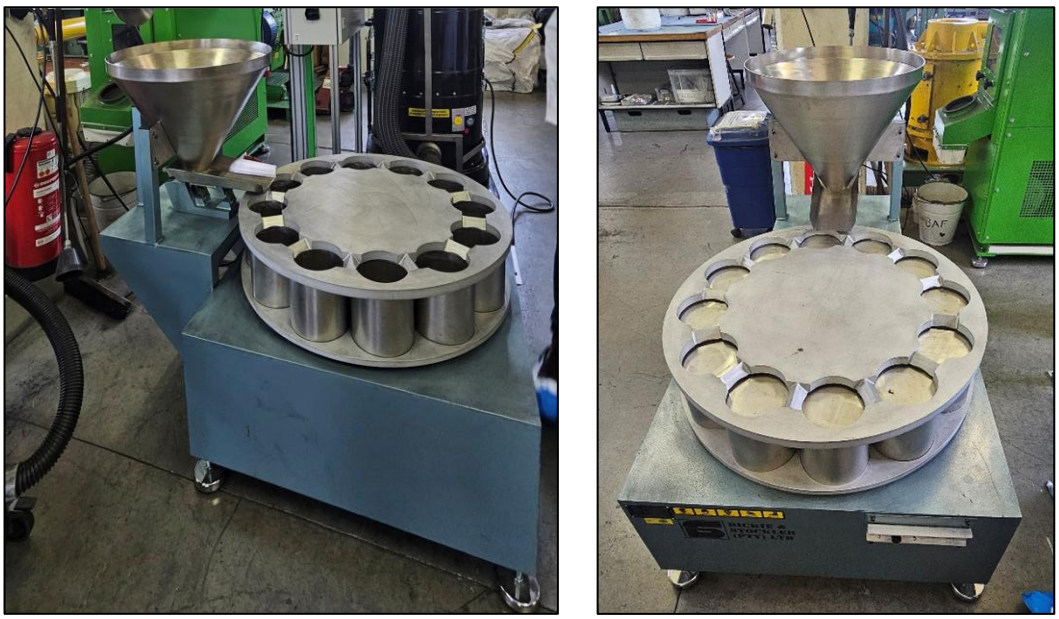


Figure 8. Dickie & Stockler 30 L 12-way Divider: Front and Side Views

ICP-OES

The elemental composition of the sub-samples was determined by inductively coupled plasma optical emission spectrometry (ICP-OES). In this method, the dissolved sample is introduced into a high-temperature argon plasma, which excites the elements to emit light at characteristic wavelengths. The emitted intensities are measured and converted to elemental concentrations. Hydrochloric acid (HCl) and nitric acid (HNO_3) were used in a ratio of 1:3. [7]

Aluminum reacts strongly with acids, requiring careful control of sub-sample mass relative to digestion vessel volume during microwave digestion, in order to prevent excessive pressure and temperature rise. Initial experiments used 300 mg sub-samples for model materials. Following the acquisition of larger digestion vessels, sample masses were adjusted to 500 mg for fractions above 2 mm and 1 g for fractions above 0.25 mm. Real foil fraction samples were digested at 1 g.

Haver & Boecker EML Digital Plus

To determine the particle size distribution of the real foil fractions, sieve analysis was performed using a Haver & Boecker EML Digital Plus sieve shaker. The instrument was operated at an amplitude of 1.0 mm, an interval setting of 10, and a sieving time of 20 minutes per run.

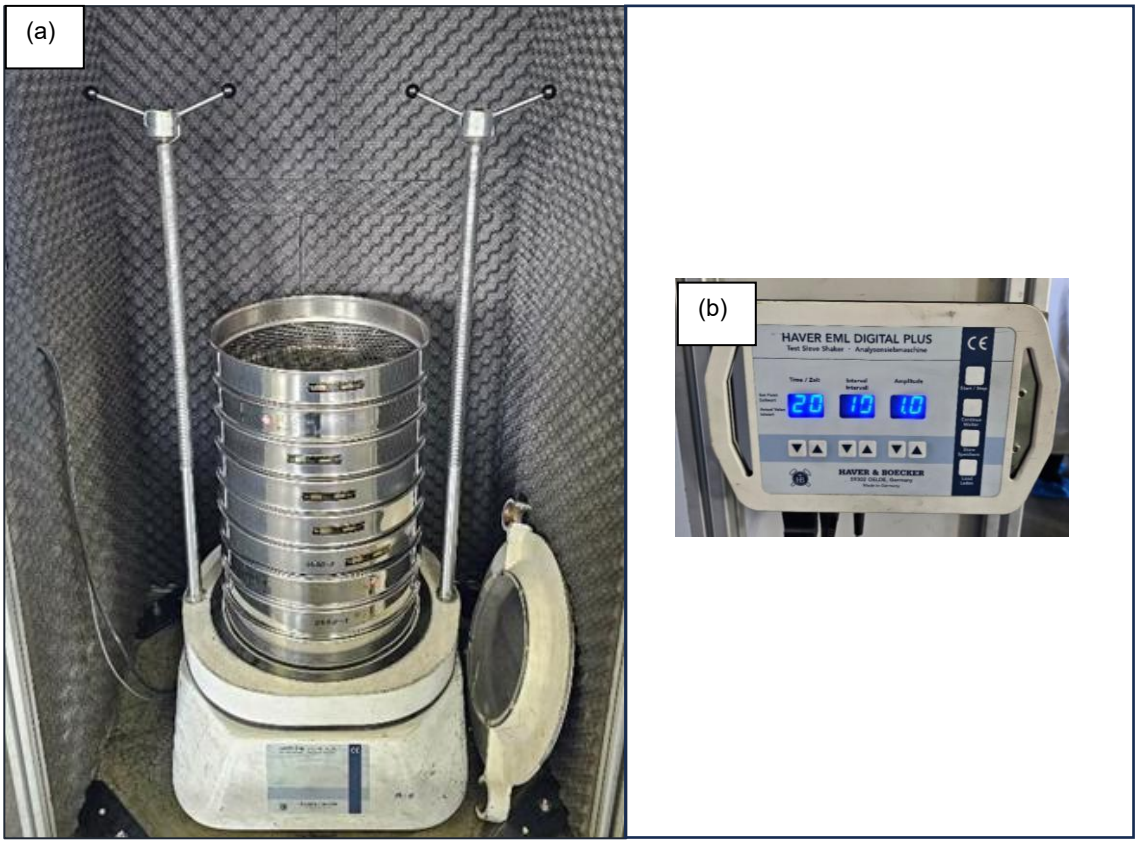


Figure 9. (a) Haver & Boecker EML Digital Plus sieve shaker with stacked sieve tower for particle size separation. (b) Digital control panel showing settings and operation parameters.

3.2. Methodology

The main experimental workflow consisted of three steps: sample preparation, two-step crushing by ShredCat, and sample splitting by DS rotary splitter prior to ICP-OES analysis. In total, 21 experiments were conducted across three main parts, producing 166 individual sub-samples for ICP-OES analysis. The first part used model material to evaluate the ShredCat method. The second part compared manual sorting to the ShredCat method. The third part applied ShredCat to real foil fractions from different cell types. One additional real foil fraction sample was used for PSD analysis only. Sieve analysis was performed using sieve sizes ranging from 0.25 mm to 12.5 mm with the Haver & Boecker EML Digital Plus sieve shaker.

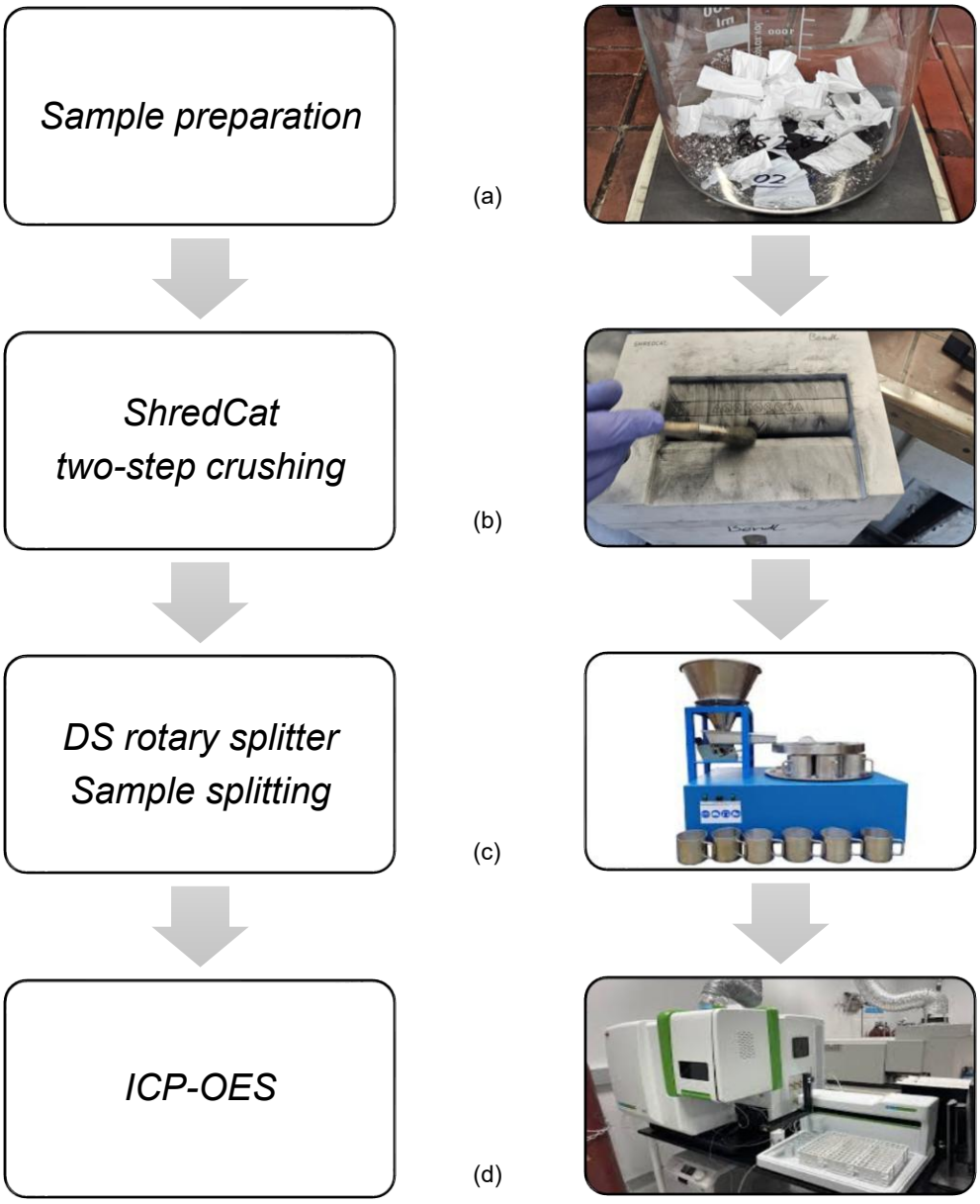


Figure 10. Main experiment flow chart (a) model material preparation (b) crushing process (c) DS rotary splitter. Source: rseprojects.co.za (d) ICP-OES equipment set-up. Source: eal.ucmerced.edu

3.2.1. Model material analysis

The model material was prepared in three particle size fractions: above 4 mm, above 2 mm, and above 0.25 mm, according to Table 2. The mass composition of each fraction was taken from previous studies. Each experiment was prepared by weighing all components of the model material, namely Al foil, Cu foil, separator, and BM, and mixing them in a beaker (Fig. 4). The mixed model material was then processed through two-step crushing by ShredCat, after which the material was split using the DS rotary splitter, producing 12 sub-samples. Eight of the 12 sub-samples from each experiment were submitted for ICP-OES analysis, and the reported elemental concentrations represent the average of those 8 sub-samples.

A total of twelve experiments were performed in this part, yielding 96 sub-samples analyzed by ICP-OES. The target mass per sub-sample was initially 300 mg for all fractions, and was subsequently revised to 500 mg for fractions above 2 mm and 1 g for fractions above 0.25 mm, following the availability of larger acid digestion vessels for microwave ICP-OES.

3.2.2. Manual sorting vs ShredCat

This part of the study used real foil fraction material remaining from previous manual sorting experiments. The same experimental workflow was applied across 6 experiments, with a target mass per sub-sample of 1 g. Five experiments generated 8 sub-samples each, while one experiment produced 6 sub-samples due to insufficient sample mass, resulting in a total of 46 sub-samples analyzed by ICP-OES. The results were compared against the manual sorting results from the same material in terms of elemental composition.

3.2.3. Real foil fractions with different cell types

The third part involved analyzing real foil fractions from three different cell types: one pouch cell and two prismatic cell types. The same experimental workflow was applied across 3 experiments, producing 24 sub-samples for ICP-OES analysis, with a target mass per sub-sample of 1 g.

4. Results

In this thesis, a total of 22 experiments were conducted which divided into 21 having ICP analysis and 1 having PSD analysis. Each experiment depending on the mass of samples, required around 3 to 4 hours.

4.1. Model material analysis

The three different particle sizes were examined to determine whether size classification for larger particle size fractions was necessary before the two-step crushing.

Table 5. Mass loss comparison of three foil fraction sizes

Particle size fractions	Mass before crushing	Mass after crushing	Mass loss	
	$m_0\ [g]$	$m\ [g]$	$[g]$	$[wt.-\%]$
> 0.25 mm	100.09	96.27	3.82	3.82
> 2 mm	40.09	38.28	1.81	4.51
> 4 mm	25	23.69	1.31	5.24

To calculate the mass loss, Eq. (9) and Eq. (10) were used.

Mass loss in grams – absolute mass loss:

$$Mass\ loss = \Delta m\ (g) = m_0 - m \tag{9}$$

Mass loss in wt.-% – percentage mass loss:

$$Mass\ loss\ (\%) = \frac{\Delta m}{m_0} \cdot 100\% \tag{10}$$

An example calculation: mass loss of > 0.25 mm fraction size

$$Mass\ loss\ (g) = \Delta m = m_0 - m = 100.09\ g - 96.27\ g = 3.82\ g$$

$$Mass\ loss\ (\%) = \frac{\Delta m}{m_0} = \frac{3.82\ g}{100.09\ g} \cdot 100 = 3.82\ wt.-\%$$

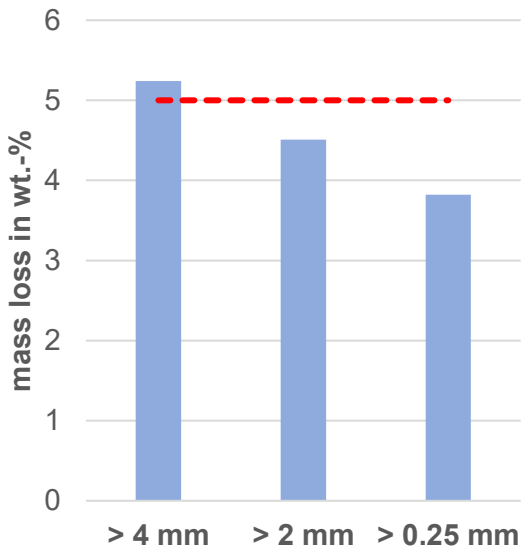


Figure 11. Mass loss comparison across foil fractions

As shown in Figure 11, the mass loss of the > 4 mm particle size fraction was 5.24 wt.-% which was higher than acceptable limit of 5 wt.-%. Therefore, further experiments included the > 2 mm and > 0.25 mm particles size fractions.

During the experiment, ShredCat_1 broke down after 4 experiments due to engine overheating. Investigation identified that BM accumulated inside the shredder, as BM dust was found in the internal components as shown in Figure 12. This indicated that BM was being selectively lost during crushing. Based on this finding, ShredCat_2 had the internal modification described in materials section. Since ShredCat_1 broke down before repeat experiments could be performed, no average or error bar is reported for its values, and error bars are not reported for the ShredCat_1 values.

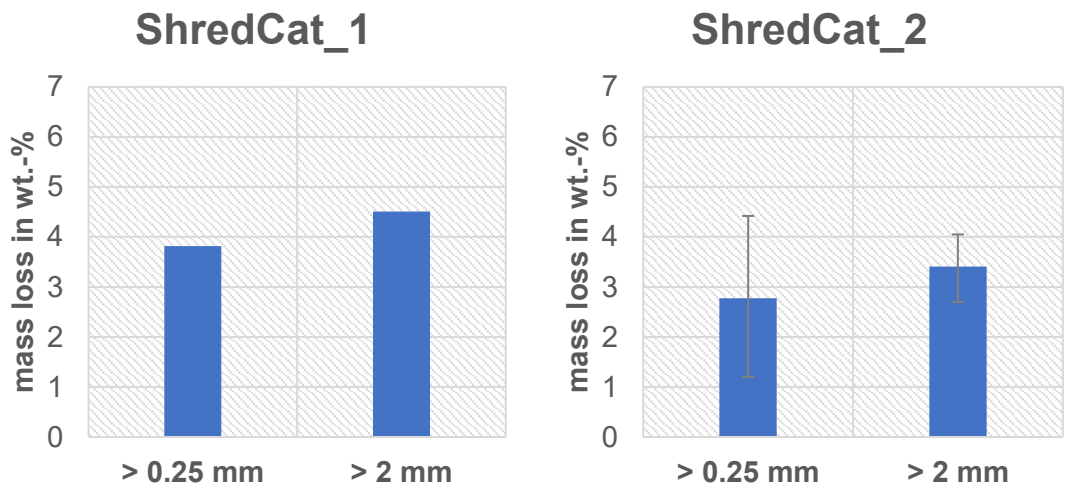


Figure 12. Comparative mass loss in ShredCat_1 and ShredCat_2

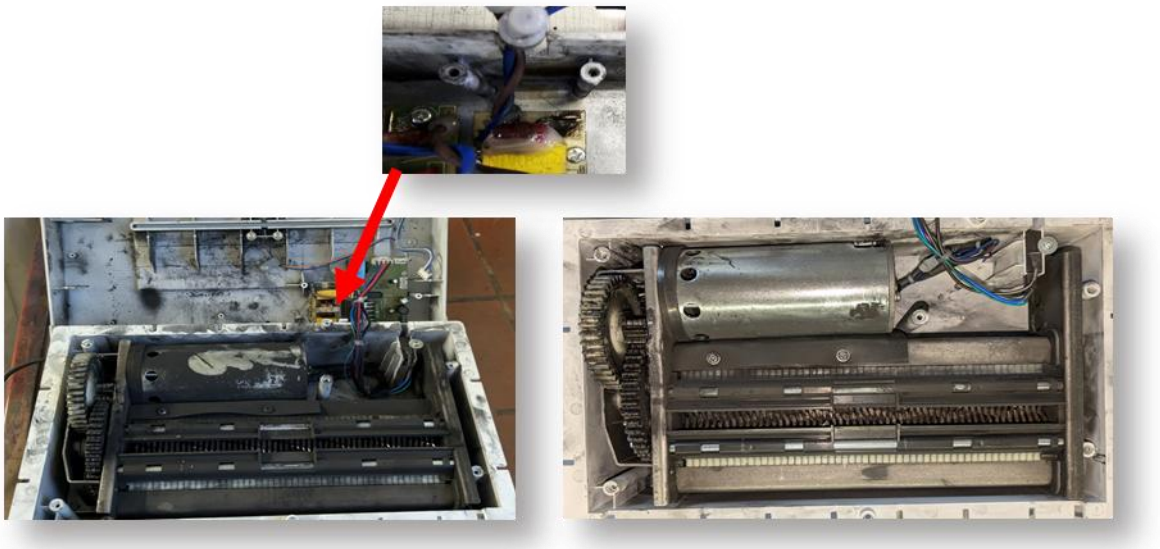


Figure 13. ShredCat_1: pre-cleaning and post-cleaning state

The above 2 mm fraction analysis was repeated 3 times, and the above 0.25 mm fraction analysis was repeated 5 times; the data for both are given in Table 6. For analyses within the same particle size group, the absolute average was used rather than the simple average, since individual values include both positive and negative deviations, and the absolute average provides a more representative summary of the overall measurement error.

The elemental content of the model material components was established prior to the experiments and is given in Table 3. The elemental content after ShredCat processing was calculated according to Eqs. (1) and (3). The relative difference in elemental content, expressed in wt.-%, between the initial composition and the ICP-OES measurement after ShredCat processing was calculated for each element, namely Al, Cu, CAM, and Rest, according to Eq. (11).

$$\Delta c_{element}(\%) = \frac{c_{element,ICP} - c_{element,model}}{c_{element,model}} \quad (11)$$

$$Average = m(X) = \frac{\sum_{j=1}^{n} x_j}{n} \quad (12)$$

$$Absolute\ average = \frac{1}{n}\sum_{j=1}^{n}\left|x_j - m(X)\right| \quad (13)$$

An example calculation of the relative wt.-% difference for Al in the first experiment of the above 0.25 mm fraction is provided below, and the same calculation method was applied throughout Table 6.

$$\Delta c_{Al}(\%) = \frac{c_{element,ICP} - c_{element,model}}{c_{element,model}} = \frac{22.37\% - 20.00}{20.00\%} \approx 12\%$$

An example calculation of the CAM content for the above 0.25 mm average and absolute average is also provided below.

$$Average = m(X) = \frac{0\% + 1\% - 1\% - 9\% - 3\%}{5} = -2.40\%$$

$$Absolute\ average = \frac{|0| + |1| + |-1| + |-9| + |-3|}{5} = 2.80\%$$

Table 6. Relative wt.-% difference between ShredCat method's ICP-OES elemental composition and model material composition in Table 3

	Al		Cu		CAM		Rest	
	> 2 mm	**> 0.25 mm**	**> 2 mm**	**> 0.25 mm**	**> 2 mm**	**> 0.25 mm**	**> 2 mm**	**> 0.25 mm**
1	31%	12%	32%	9%	-16%	0%	-5%	-15%
2	9%	10%	24%	10%	-12%	1%	-1%	-16%
3	17%	19%	16%	11%	-15%	-1%	0%	-20%
4	-	10%	-	15%	-	-9%	-	-9%
5	-	12%	-	10%	-	-3%	-	-12%
Average	19.00%	12.60%	24.00%	11.00%	-14.33%	-2.40%	-2.00%	-14.40%
Absolute average	19.00%	12.60%	24.00%	11.00%	14.33%	2.80%	2.00%	14.40%

As shown in Figure 14, the results consistently indicate that Al and Cu increased in relative wt.-% while CAM and Rest decreased, for both particle size fractions. However, the magnitude of the deviations was large, suggesting that a simple relative wt.-% comparison is insufficient to fully account for the compositional measurement. Further analysis was therefore carried out using correction estimations aimed at reducing the relative wt.-% deviation.

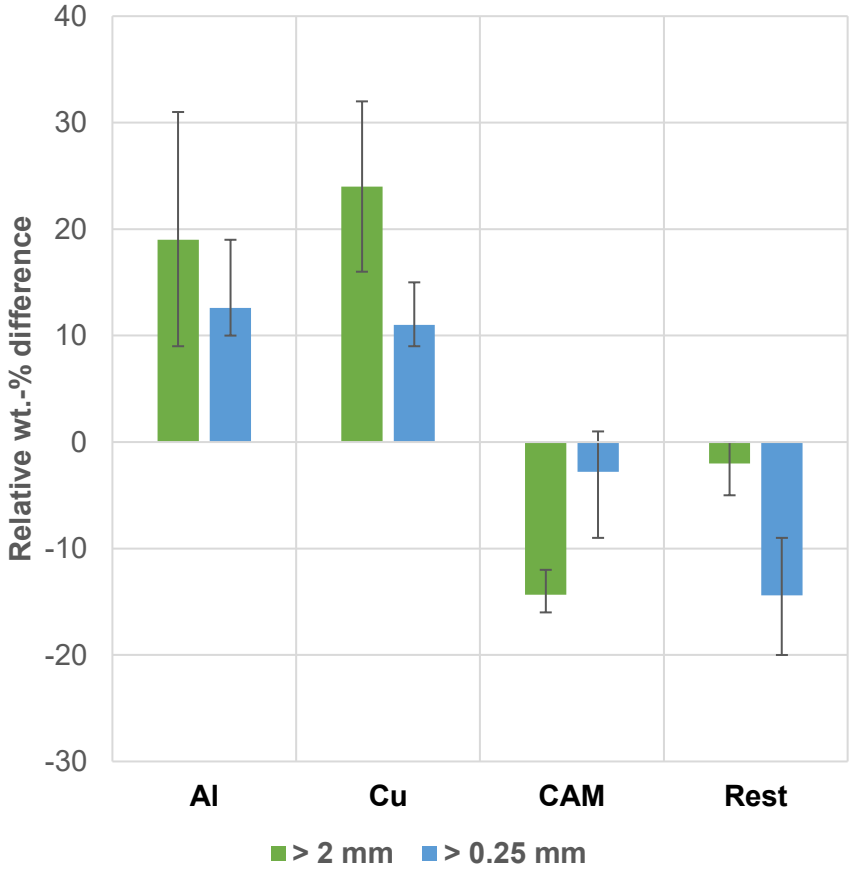


Figure 14. Comparison of relative wt.-% difference for each element between the calculated model material composition and the ShredCat analysis results

Despite the ShredCat_2 modification reducing mass loss, measurable mass loss was still detected. Additionally, BM dust loss was observed during sample splitting. Two correction estimations were therefore applied: in the first, BM loss was assumed to occur during crushing only; in the second, BM loss was assumed to occur during both crushing and splitting. The measured ICP-OES results served as the baseline for both correction estimations.

Correction formula for two estimations:

$$\Delta c_{element,est_1} = \frac{c_{element,ICP} - c_{element,corrected\ by\ ShredCat}}{c_{element,corrected\ by\ ShredCat}} \quad (13)$$

$$\Delta c_{element,est_2} = \frac{c_{element,ICP} - c_{element,corrected\ by\ BM\ only}}{c_{element,corrected\ by\ BM\ only}} \quad (14)$$

Table 7. Corrected wt.-% composition of elements following first estimation

	Al		Cu		CAM		Rest	
	> 2 mm	**> 0.25 mm**	**> 2 mm**	**> 0.25 mm**	**> 2 mm**	**> 0.25 mm**	**> 2 mm**	**> 0.25 mm**
1	26%	7%	20%	5%	-9%	5%	-2%	-13%
2	6%	8%	27%	8%	-12%	4%	-6%	-15%
3	13%	16%	12%	9%	-9%	5%	-1%	-20%
4	-	7%	-	11%	-	-5%	-	-8%
5	-	11%	-	9%	-	-2%	-	-12%
Average	15.00%	9.80%	19.67%	8.40%	10%	0.85%	-3.00%	-13.60%
Absolute average	15.00%	9.80%	19.67%	8.40%	10%	3.6%	3.00%	13.60%

Applying the first correction, which assumes BM loss occurs during crushing only, Al and Cu showed positive relative wt.-% differences while CAM and Rest showed negative relative differences for both size fractions. Despite this directional split, all components moved closer to zero, indicating a reduction in deviation.

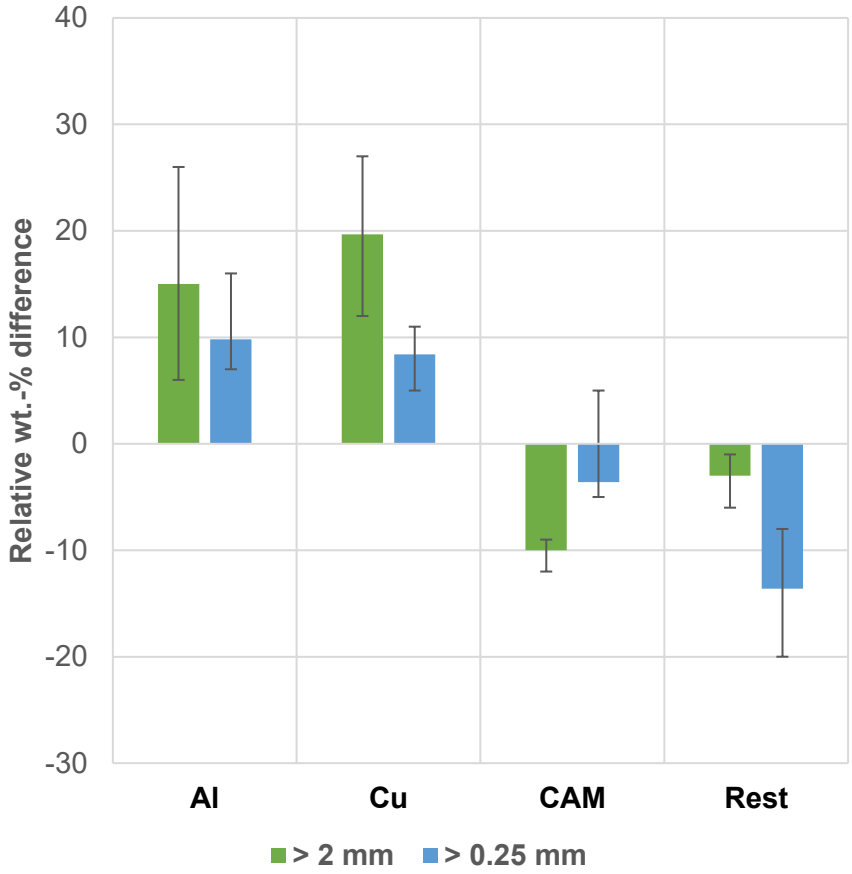


Figure 15. Comparison of relative wt.-% difference for each element between the measured ShredCat analysis results and the refined composition after first estimation correction

Table 8. Corrected wt.-% composition of elements following second estimation

	Al		Cu		CAM		Rest	
	> 2 mm	> 0.25 mm	> 2 mm	> 0.25 mm	> 2 mm	> 0.25 mm	> 2 mm	> 0.25 mm
1	9.0%	7%	8.3%	0%	-3.8%	12%	-2.2%	-18%
2	-	-4%	-	0%	-	8%	-	-4%
3	-	4%	-	2%	-	5%	-	-10%
Average	-	2%	-	1%	-	8%	-	-11%
Absolute average	-	5%	-	1%	-	8%	-	11%

Applying the second correction, which accounts for the selective mass loss of BM during both the crushing and splitting stages, reduced the deviation in the same general pattern as observed under the first correction, with improvements seen across all components and size fractions. However, the second correction produced the lowest values across all components and size fractions when compared to both the uncorrected

data and the first correction, indicating that accounting for BM loss at both processing stages yields the greatest overall reduction in deviation.

Throughout both corrections, the above 0.25 mm fraction consistently exhibited the lowest deviations and remained closest to zero across all components. One exception was observed: the CAM content in the above 0.25 mm fraction showed an increased deviation under the second correction, diverging from the trend seen in all other components and size fractions. This was the only instance in which applying the second correction resulted in a higher deviation compared to the first correction.

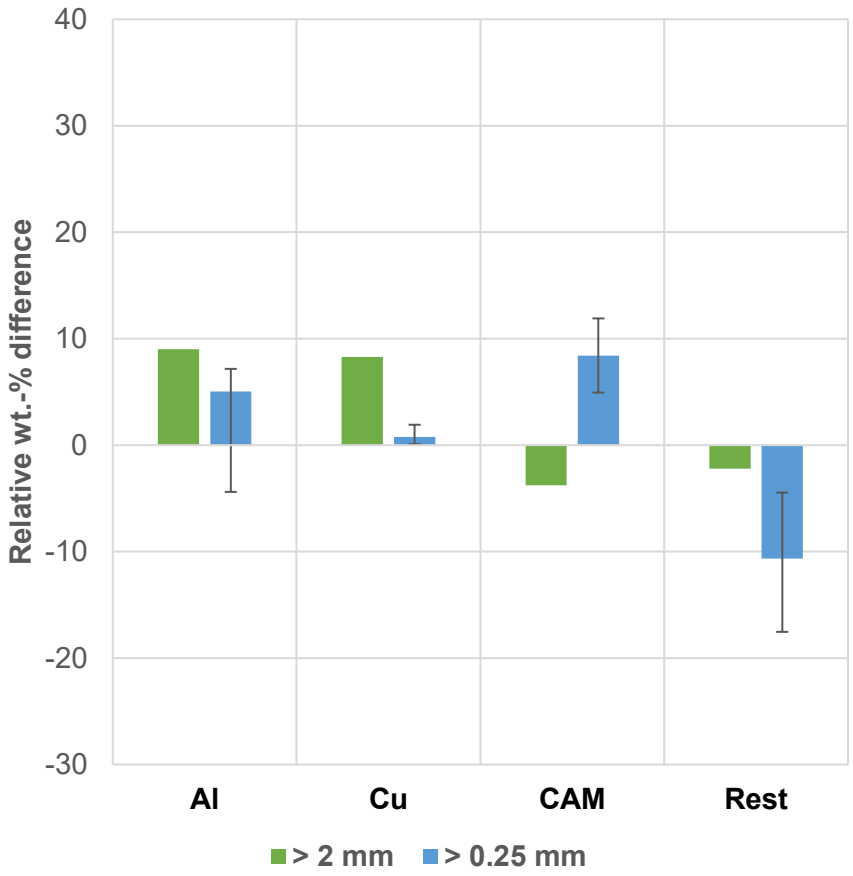


Figure 16. Comparison of relative wt.-% difference for each element between the measured ShredCat analysis results and the refined composition after second estimation correction

4.2. Manual sorting vs ShredCat

The average mass loss across the 6 experiments was 3.19 wt.-%, of which approximately 2.00 wt.-% occurred during crushing and 1.19 wt.-% during splitting.

Table 9. Relative wt.-% difference: manual sorting vs ShredCat analysis

№	Al	Cu	CAM	Rest
1	-15%	-85%	-32%	33%
2	-13%	-85%	-34%	33%
3	-12%	-77%	-34%	34%
4	-20%	-15%	-20%	25%
5	-13%	9%	11%	-1%
6	18%	-18%	-14%	19%

The relative wt.-% differences between manual sorting and ICP-OES measurements revealed distinct patterns across the experiments. Experiments 1 to 3, which used air classification products, showed consistent negative deviations for Al (−12% to −15%), Cu (−77% to −85%), and CAM (−32% to −34%), with corresponding positive deviations for the Rest fraction (33% to 34%). The similarity of these trends across all three experiments reflects the compositional uniformity expected from a single air classification operation.

Experiments 4 and 5, which used sieving-based products, exhibited markedly different deviation patterns: Al values ranged from −20% to −13%, Cu showed a wide range from −15% to 9%, CAM varied from −20% to 11%, and Rest ranged from −1% to 25%. These variations, and the overall magnitude of the deviations, differ substantially from the air-classified samples, reflecting the distinct separation characteristics of sieving compared to air classification.

4.3. Real foil fractions with different cell types

The total mass loss for the three real foil fraction experiments was lower than that observed in the model material experiments. Prismatic cell 1 showed the highest total mass loss at 2.75 wt.-%, with 1.73 wt.-% occurring during crushing and 1.03 wt.-% during splitting. Prismatic cell 2 and the pouch cell showed lower total mass losses of 1.23 wt.-% and 1.31 wt.-% respectively.

The elemental compositions of the three fractions are presented in Table 10. Cu showed the largest variation between cell types, ranging from 21.67 wt.-% in Prismatic cell 2 to 28.46 wt.-% in Prismatic cell 1. Al showed less variation, ranging from 17.67 wt.-% in Prismatic cell 1 to 23.92 wt.-% in Prismatic cell 2. CAM and Rest remained relatively consistent across all three cell types, while Fe showed consistently low values across all

fractions. The pouch cell showed the highest Rest concentration at 32.97 wt.-%, compared to 29.99 wt.-% and 29.86 wt.-% for Prismatic cells 1 and 2 respectively.

Table 10. Elemental wt.-% composition by cell type

Cell types	Al	Cu	Fe	CAM	Rest
Prismatic 1	17.67	28.46	0.11	21.90	29.99
Prismatic 2	23.92	21.67	0.14	22.17	29.86
Pouched	21.96	22.28	0.45	20.32	32.97

Table 11. Particle size distribution (PSD) analysis of after-ShredCat real foil fraction

Class		**Mass**	**Mass fraction**	**Cumulative distr.**		**Class width**	**Distr. density**
$x\ [mm]$		$m_{3,i}\ [g]$	$\mu_{3,i}\ [\%]$	$Q_{3,i}(x)\ [\%]$	$R_{3,i}(x)\ [\%]$	$\Delta x_i\ [mm]$	$q_{3,i}(x)\ \left[\frac{\%}{mm}\right]$
12.5	-	0	-	-	-	-	-
10	12.5	0.2	0.13	100	0	2.5	19.85
8	10	0.3	0.19	99.87	0.13	2	10.59
4	8	10.6	6.68	99.69	0.31	4	0.60
3.15	4	6.4	4.03	93.01	6.99	0.85	0.21
2	3.15	16.2	10.20	88.98	11.02	1.15	0.11
1	2	56.7	35.71	78.78	21.22	1	0.03
0.5	1	37.5	23.61	43.07	56.93	0.5	0.02
0.315	0.5	2	1.26	19.46	80.54	0.185	0.15
0.25	0.315	1.2	0.76	18.20	81.80	0.065	0.09
0	0.25	27.7	17.44	17.44	82.56	0.25	0.01
Total, m_t		158.8	100	0	100	-	-

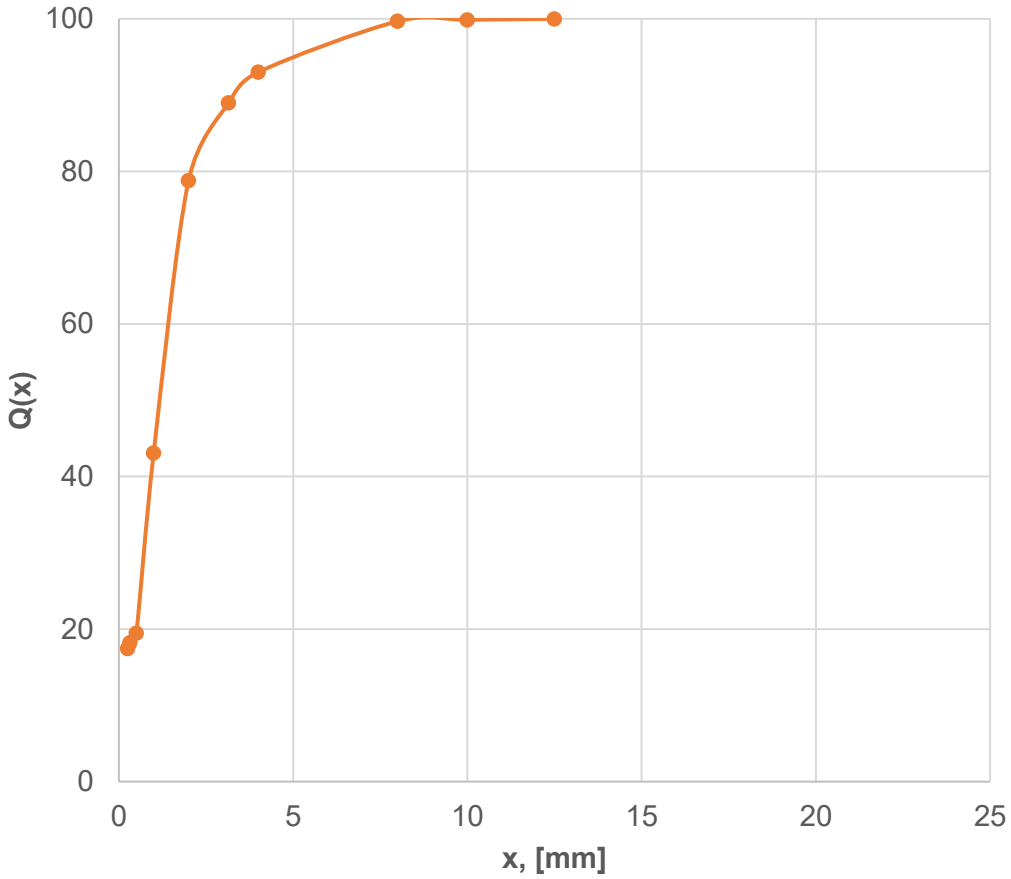


Figure 17. Cumulative particle size distribution (PSD) curve of after-ShredCat real foil fraction

5. Discussion

The above 4 mm fraction was discontinued after the initial 3 experiments, as it produced the highest mass loss, exceeding 5 wt.-%. This indicated that the coarser fraction was not well suited to the ShredCat method for model material, as the material could not be sufficiently processed without excessive loss.

The ShredCat modification proved effective in reducing BM loss. For the above 2 mm fraction, total mass loss decreased from 4.51 wt.-% to 3.41 wt.-%, and for the above 0.25 mm fraction from 3.82 wt.-% to 2.77 wt.-%, following the introduction of the 3D-printed connector. This confirms that the loss point identified between the cross-cutter and the feed inlet was a significant source of BM dust loss, and that the modification successfully reduced it.

The two correction estimations consistently moved all relative wt.-% differences closer to zero, with the second correction, which accounts for BM loss during both crushing and splitting, producing the lowest deviations across all components and both size fractions. This suggests that BM loss occurs across both processing steps, and that accounting for splitting loss in addition to crushing loss improves the accuracy of the compositional estimation. The above 0.25 mm fraction consistently showed the smallest deviations throughout, indicating that the ShredCat method performs better without pre-sieving and that processing the fraction as a whole is the more effective approach.

The exception observed for CAM in the above 0.25 mm fraction under the second correction, where deviation increased rather than decreased, may be attributed to overcorrection. As the second correction applies a larger BM loss assumption, it is possible that the assumed loss exceeded the actual loss for CAM in this fraction, shifting the corrected value past zero in the opposite direction. This suggests that BM loss may not be distributed uniformly across all components, and that fraction-specific correction factors may be needed for further refinement of the method.

The average total mass loss of 3.19 wt.-%, with 2.00 wt.-% attributed to crushing and 1.19 wt.-% to splitting, confirms that crushing is the dominant source of material loss in the ShredCat method. The relatively small splitting loss suggests that the DS rotary splitter introduces minimal additional loss to the process.

The relative wt.-% differences between manual sorting and ICP-OES measurements revealed distinct and systematic patterns across the experiments. Experiments 1 to 3, conducted on air classification products, showed consistent negative deviations for Al, Cu, and CAM, with corresponding positive deviations for the Rest fraction across all three experiments. The consistency of these trends reflects the compositional uniformity

expected from a single air classification operation, and confirms that the observed differences are systematic rather than the result of random variation.

Experiments 4 and 5, conducted on sieving-based products, exhibited markedly different deviation patterns, with wider ranges and substantially different magnitudes compared to the air-classified samples. This divergence is attributed to the distinct separation characteristics of sieving versus air classification, which produce foil fractions of different composition and particle size distribution.

Experiment 6 also used an air classification product foil fraction; however, it differed from Experiments 1 to 3 in that the separator contained an Al_2O_3 coating. This distinction had a notable effect on the measured composition, as Experiment 6 recorded the highest Al content among all experiments. It is important to note that this elevated Al concentration is not primarily attributable to the aluminum foil itself, but rather originates predominantly from the Al_2O_3 coating on the separator, which contributes additional Al upon dissolution during ICP-OES analysis. The origin and pre-treatment of the samples therefore play a significant role in the deviation patterns observed between manual sorting and the ShredCat method, and comparisons across samples of different origins should be made with caution.

The consistent negative deviation for Cu in the air-classified samples, and its wide variation in the sieving-based samples, suggests that the recoverability of Cu is sensitive to the physical form of the material. Since Cu is visually distinguishable, manual sorting may systematically over-recover it in certain sample types, whereas the ShredCat method measures elemental concentration directly, regardless of particle form. The foil fraction is a fibrous material in which the shredding process substantially increases particle surface area, which may enhance chemical reactivity during ICP-OES sample preparation and allow components enclosed within composite particles to be more completely dissolved and measured than would be possible through manual sorting.

The total mass loss observed across the three real foil fraction experiments was lower than that recorded for the model material experiments. This is consistent with the physical nature of the two material types. In the model material, BM was present as a free powder component, making it highly susceptible to loss during crushing and splitting. In real foil fractions, however, the active coating material is closely adhered to the separator foils and largely enclosed within composite electrode structures, resulting in considerably less free dust and consequently lower mass loss during processing. Among the three cell types, Prismatic cell 1 showed the highest total mass loss at 2.75 wt.-%, while Prismatic cell 2 and the pouch cell showed lower losses of 1.23 wt.-% and 1.31 wt.-% respectively.

A particle size distribution analysis was performed before and after ShredCat processing to evaluate the effect of comminution on the real foil fractions. Before processing, the maximum particle size was 25 mm, and the dominant size class was 1 – 2 mm. After ShredCat processing, the maximum particle size was reduced to 12.5 mm, indicating that the shredder effectively decreased the coarse end of the particle size distribution. In addition, a fines fraction of 17.4 wt.-% was generated at 0.25 mm, while the fraction above 4 mm decreased by approximately 3 wt.-%, confirming that the material was shifted toward smaller particle sizes during processing. The dominant 1 – 2 mm class remained the largest fraction in both datasets, with a similar share of approximately 32 – 36 wt.-%. However, the sub-0.5 mm fraction cannot be directly compared between the two datasets because the pre-processing sample was not sieved below 0.5 mm. Overall, the results show that ShredCat processing achieved sufficient comminution for representative sub-sampling.

The elemental compositions of the three cell types showed clear differences, particularly for Cu and Al, confirming that different cell types and origins produce foil fractions with distinct compositions. Cu showed the largest variation between cell types, while CAM and Rest remained relatively consistent across all three. These findings have direct practical implications: a single reference composition cannot be reliably applied across different cell types, and cell-type-specific reference values are necessary for accurate compositional determination using the ShredCat method.

Taken together, the results across all three experimental parts support the conclusion that the ShredCat method is a viable alternative to manual sorting for analyzing the coarse foil fraction of LIBs. The method produces consistent and reproducible results, the correction estimations demonstrate a clear and logical response to BM loss, and the systematic trends observed in the manual sorting comparison confirm that the ShredCat method captures compositional information reliably. Further refinement of the correction factors, particularly with regard to fraction-specific behavior, would strengthen the method and improve its quantitative accuracy.

6. Conclusion

The rapid growth of the electric vehicle market and tightening European Union material recovery targets have made the efficient, scalable recycling of LIBs an absolute necessity. While mechanical pre-treatment routinely successfully isolates the fine black mass fraction, the compositional characterization of coarser, larger particle size fractions (0.25 mm to 20 mm) has been bottlenecked by manual sorting. Manual sorting is severely limited by low throughput, susceptibility to human error, and a restriction to small sample masses, leaving a distinct methodological gap in recycling process development.

This thesis successfully validated an alternative analytical method combining mechanical comminution via a modified ShredCat paper shredder, DS rotary splitter, and ICP-OES analysis. The experimental validation yielded several key insights across the model materials, manual sorting benchmarks, and real foil fractions:

- *Method feasibility and mass loss mechanics*: Processing materials through the ShredCat system resulted in a low and manageable average total mass loss of 3.19 wt.-%. Comminution was identified as the primary source of material loss (accounting for 2.00 wt.-%), while the DS rotary splitter introduced minimal additional dust loss (1.19 wt.-%). Furthermore, real foil fractions exhibited lower mass losses than the model materials. This is highly advantageous and is attributed to the fact that active material in real battery scrap is closely adhered to separator foils and enclosed within composite structures, rather than existing as highly transportable free powder.
- *Optimal processing sizing*: Among the tested particle size boundaries, the coarser above 4 mm fraction was discontinued due to excessive dust generation exceeding 5 wt.-%. Conversely, the above 0.25 mm fraction consistently demonstrated the smallest analytical deviations. This indicates that the ShredCat method performs optimally without the need for pre-sieving, allowing the coarse fraction to be treated directly as a whole.
- *Correction and system modifications*: Mechanical engineering interventions — specifically the installation of a custom 3D-printed connector body between the cross-cutter and the feed inlet — successfully minimized black mass dust escape, reducing total mass loss for the 0.25 mm fraction from 3.82 wt.-% to 2.77 wt.-%. Applying a two-step mathematical estimation correction that accounts for cumulative black mass losses during both crushing and splitting successfully minimized relative wt.-% deviations, bringing analytical outcomes closest to the true expected baseline model material compositions.

- *ShredCat vs manual sorting benchmarks*: A comparative analysis against manual sorting data revealed distinct, systematic patterns. Manual sorting was shown to systematically under-recover critical metals and active material components relative to the ShredCat method, particularly within air-classified process streams. Because the shredding process substantially increases the exposed particle surface area, it enhances chemical dissolution during ICP-OES sample preparation. This allows embedded metallic elements tightly bound within complex composites to be thoroughly liberated and quantified, bypassing the visual and physical classification boundaries of human handling.
- *Cell-type heterogeneity*: Evaluating distinct real scrap profiles confirmed that elemental composition varies considerably depending on the original battery architecture and cell chemistry. Notably, copper content showed the widest variation between pouch and prismatic cells. Additionally, pre-treatment indicators such as aluminum oxide (Al_2O_3) separator coatings can substantially shift element footprints, for example by artificially elevating total Al readings during chemical analysis. Consequently, applying a single reference composition across mixed waste streams is fundamentally unviable, reinforcing the need for cell-type-specific baseline parameters.

In summary, this research demonstrates that the ShredCat and ICP-OES method represents a highly viable, reproducible, and scalable alternative to manual sorting. By mitigating the throughput constraints of human labor, this approach enables researchers and recycling operators to confidently analyze significantly larger sample masses. Ultimately, this provides a more representative, statistically robust method for monitoring industrial-scale material streams, establishing mass balances, and optimizing mechanical separation units to achieve the circular economy criteria demanded by modern environmental legislation.

7. Future Work

To further develop this analytical framework, future research should focus on several key areas.

- *Fraction-Specific Correction Factors*: Improve the current mathematical correction models to better represent non-uniform black mass distribution across different metallic matrices. This will help reduce the risk of localized overcorrection and improve overall accuracy.
- *Automated Inline Cleaning*: Explore mechanical and pneumatic design improvements within the cutter housing to reduce material hold-up. These changes could also improve processing efficiency.
- *Database Expansion*: Develop a more comprehensive, cell-type-specific reference database that includes a wider range of commercial EV battery cells, such as high-nickel NMC variants and LFP chemistries. This would help standardize baseline inputs when working with mixed feedstocks.

References

[1] A. K. &. J. D. (Eds), Recycling of Lithium-Ion Batteries: LithoRec Way, Cham: Springer, 2018.

[2] T. L. J. D. K. J. M. W. H. A. K. Christian Hanisch, "Recycling of lithium-ion batteries: a novel method to separate coating and foil of electrodes," *Journal of cleaner production,* vol. 108, no. Part A, pp. 301-311, 2015.

[3] C. W. A. V. U. A. P. Alexandra Kaas, "Evaluating the influence of discharge depths of lithium-ion batteries on the mechanical recycling process," *Cleaner Production,* vol. 486, 2025.

[4] M. T. Y. P. Chengetai Portia Makwarimba, "Assessment of recycling methods and processes for lithium-ion batteries," *iScience,* vol. 25, no. 5, 2022.

[5] A. Kaas, "Innovations in Mechanical Recycling of automotive Lithium-Ion Batteries: A Focus on Discharge Depths and Material Classification [Innovationen im Recycling von Lithium-Ionen-Batterien aus Elektrofahrzeugen: fokussierend]," Freiberg, 2025.

[6] Z.-Y. G. E. H. A. X.-X. Z. X.-L. W. Y. L. Xiao-Tong Wang, "Prospects for managing end-of-life lithium-ion batteries: Present and future," *Interdisciplinary Research of Materials and Energy in Honor of Nobel Laureate John B. Goodenough,* vol. 1, no. 3, 2022.

[7] C. Wilke, "Influences of different pre-treatments, settings and cell types on the first process stage of a mechanical recycling process for automotive lithium-ion batteries," Freiberg, 2025.

[8] S. Mudgil, "Parameter study on a vacuum shredder system with integrated drying to investigate the recycling quality of lithium-ion batteries (LIBs)," Freiberg, 2025.

[9] S. H. V. U. O. A. Buwa Ruturaj Rajendra, "Investigation Of Two Process Strategies for Separator Recovery in The Lithium-Ion Battery (LIB) Recycling Process," Freiberg, 2025.

[10] T. M. U. A. P. Alexandra Kaas, "Review on Zigzag Air Classifier," *Processes,* 2022.

[11] A. K. C. S. T. H. U. P. Peter Bischoff, "Fast and Efficient Evaluation of the Mass Composition of Shredded Electrodes from Lithium-Ion Batteries Using 2D Imaging," *J. Imaging,* vol. 9, no. 7, 2023.

[12] C. W. J.-S. R. T. M. U. A. P. Alexandra Kaas, "Modelling the Sorting of Lithium-Ion Battery Components in a Zig-Zag Air Classifier," *Metals,* vol. 14, no. 3, 2024.

[13] C. W. A. V. U. A. P. Alexandra Kaas, "Influence of the Cell Type on the Physical Processes of the Mechanical Recycling of Automotive Lithium-Ion Batteries," *Metals,* vol. 13, no. 11, 2023.

[14] D. M. W. A. K. U. A. P. Christian Wilke, "Influence of the Crusher Settings and a Thermal Pre-Treatment on the Properties of the Fine Fraction (Black Mass) from Mechanical Lithium-Ion Battery Recycling," *Batteries,* vol. 9, no. 10, 2023.

[15] A. K. U. A. P. Christian Wilke, "Influence of the Cell Type on the Physical Processes of the Mechanical Recycling of Automotive Lithium-Ion Batteries," *Metals,* vol. 13, no. 11, 2023.

[16] A. K. A. P. Christian Wilke, "Influence of the cell type on yield and composition of black mass deriving from a mechanical recycling process of automotive Lithium-ion batteries," *Next Sustainability,* vol. 4, 2024.

[17] G. G. C. W. B. Xue Wang, "Targeting high value metals in lithium-ion battery recycling via shredding and size-based separation," *Waste Management,* vol. 51, 2016.

[18] S. v. W. Y. P. V. N. D. W. L. F. D. F. H. P. U. P. P. M. W. D. S. N. Christoph Peschel, "Comprehensive Characterization of Shredded Lithium-Ion Battery Recycling Material," *Chemistry - A European Journal,* vol. 28, no. 22, 2022.

[19] Y. H. L. G. R. F. X. Z. Y. H. Tao Zhang, "Characteristics of wet and dry crushing methods in the recycling process of spent lithium-ion batteries," *Journal of Power Sources,* vol. 240, pp. 766-771, 2013.

[20] T. M. U. A. P. Denis Manuel Werner, "Influence of Pretreatment Strategy on the Crushing of Spent Lithium-Ion Batteries," *Metals,* vol. 12, no. 11, 2022.

[21] E. A. A. K. A. e. a. Gerold, "Interrelationships between Pre-processing and Subsequent Procedures in the Recycling of Spent Lithium-ion Batteries," *Berg Huettenmaenn Monatsh,* vol. 168, p. 346–352, 2023.

[22] A. Vanderbruggen, "Lithium-Ion Battery Recycling - Influence of Recycling Processes on Component Liberation and Flotation Separation Efficiency," *ACS ES&T Engineering,* vol. 2, no. 11, 2022.

[23] A. Vanderbruggen, "Lithium-Ion Battery Recycling—Influence of Recycling Processes on Component Liberation and Flotation Separation Efficiency," *ACS ES&T Engineering,* vol. 2, no. 11, 2022.

[24] C. W. A. V. U. A. P. Alexandra Kaas, "Influence of different discharge levels on the mechanical recycling efficiency of lithium-ion batteries," *Waste management,* vol. 172, pp. 1-10, 2023.

Appendix A: Non-disclosure agreement

Verpflichtungserklärung

Ich erkläre hiermit, die Regelungen des Vertrages

Forschungs- und Entwicklungs-Kooperationsvertrag
(genaue Bezeichnung des Vertrages mit Unterschriftsdatum)

Vertragspartner: BASF Schwarzheide GmbH
(genaue Bezeichnung des Vertragspartners)

Thema: „Mechanisches Recycling von Lithium-Ionen-Batterien"
(genaue Bezeichnung des Vertragsthemas)

soweit sie mich betreffen,

- insbesondere zur Übertragung eventueller Erfindungen und Rechte an Arbeitsergebnissen, zur Vertraulichkeit und Geheimhaltung sowie zur Genehmigungspflicht etwaiger Veröffentlichungen -

gelesen und verstanden zu haben und verpflichte mich, sie zu beachten.

Der Übertragung von Erfindungen auf den Vertragspartner sowie der Einräumung von Nutzungsrechten für den Vertragspartner -wie vertraglich vereinbart- wird bereits jetzt ausdrücklich zugestimmt. Das Recht auf Vergütung und zwingende gesetzliche Regelungen bleiben unberührt.

Ich verpflichte mich gegenüber dem Vertragspartner, alle von mir gemachten Diensterfindungen gemäß § 5 ArbnErfG zu melden und die jeweiligen Erfinderanteile zu benennen.

Die Verpflichtung zu Vertraulichkeit und Geheimhaltung gilt auch nach Ausscheiden aus der TU Bergakademie Freiberg gemäß den Regelungen des Vertrages, des Arbeitsvertrages und des geltenden Tarifvertrages.

Sainzaya Odbayar
(Name, Vorname)

Agricolastr 16, 705B, 09599 Freiberg
(Hauptwohnsitz)

29.10.2025 (Ort) | Freiberg (Datum) | O. Sainzaya (Unterschrift)

Anlage: Auszug aus dem Forschungs- und Entwicklungs-Kooperationsvertrag

6. Geheimhaltung

6.1 „INFORMATIONEN" sind alle technischen, kommerziellen und geschäftlichen Informationen, einschließlich Formeln, Ideen, Muster, Dokumente, Spezifikationen, Daten sowie Materialproben die der TUBAF im Rahmen dieses Vertrages mündlich, schriftlich oder auf andere Weise mitgeteilt bzw. zugänglich gemacht werden. Zu den INFORMATIONEN im Sinne dieses Vertrages gehören auch ARBEITSERGEBNISSE.

6.2 TUBAF wird hiermit von BASF darauf hingewiesen, dass INFORMATIONEN für BASF einen wesentlichen kommerziellen Wert haben und seitens BASF durch Geheimhaltungsmaßnahmen geschützt sind.

6.3 Die TUBAF wird alle INFORMATIONEN vertraulich behandeln, Dritten nicht zugänglich machen, weder ganz noch auszugsweise vervielfältigen und sie nur für die Durchführung der VERTRAGSARBEITEN verwenden. Die TUBAF wird sicherstellen, dass die seitens der TUBAF an den VERTRAGSARBEITEN mitwirkenden Personen diese Verpflichtung einhalten.

6.4 Die TUBAF wird alle erforderlichen und geeigneten Vorkehrungen treffen, damit INFORMATIONEN jederzeit wirksam gegen Verlust sowie gegen unberechtigten Zugriff geschützt sind. Hierzu gehören insbesondere die Schaffung und Aufrechterhaltung von geeigneten und erforderlichen Zutritts- bzw. Zugriffsvorkehrungen für Räumlichkeiten, Behältnisse, IT-Systeme, Datenträger und sonstige Informationsträger, in bzw. auf denen sich INFORMATIONEN befinden. Die TUBAF verpflichtet sich, BASF unverzüglich schriftlich zu benachrichtigen, wenn ein Verlust oder ein unberechtigter Zugriff auf INFORMATIONEN eingetreten ist oder befürchtet wird.

6.5 Diese Geheimhaltungsverpflichtung gilt nicht für INFORMATIONEN,

- die der TUBAF vor Erhalt von BASF schon ohne Verpflichtung zur Geheimhaltung oder Nichtbenutzung bekannt waren,
- die öffentlich bekannt sind oder ohne Verstoß gegen diese Geheimhaltungsverpflichtung öffentlich bekannt werden,
- die der TUBAF auf rechtmäßige Weise ohne Verpflichtung zur Geheimhaltung oder Nichtbenutzung von Dritten zugänglich werden,
- in deren Weitergabe oder Bekanntmachung BASF zuvor schriftlich ausdrücklich eingewilligt hat.

INFORMATIONEN fallen nicht schon deswegen unter die oben genannten Ausnahmen, weil sie von allgemeinen Kenntnissen und Erfahrungen umfasst werden, die als solche unter mindestens eine dieser Ausnahmen fallen. Gleichermaßen fällt eine Kombination von Einzelinformationen nicht schon deswegen unter die oben genannten Ausnahmen, weil die Einzelinformationen dieser Kombination als solche unter mindestens eine dieser Ausnahmen fallen, sondern nur dann, wenn auch die Kombination selbst unter mindestens eine dieser Ausnahmen fällt.

Soweit INFORMATIONEN in einem Gerichts- oder Verwaltungsverfahren aufgrund eines Beschlusses oder einer Anordnung des Gerichts bzw. der Behörde offengelegt werden müssen, ist die TUBAF berechtigt, einer solchen Verpflichtung nachzukommen. Die TUBAF wird BASF über solche Beschlüsse oder Anordnungen unverzüglich und rechtzeitig vor der Offenlegung der INFORMATIONEN schriftlich informieren und den Empfänger bitten, die Geheimhaltung aufrecht zu erhalten.

6.6 TUBAF verpflichtet sich Materialproben, die sie im Rahmen dieses Vertrages unmittelbar oder mittelbar von BASF erhält, ausschließlich zum Zwecke der VERTRAGSARBEITEN zu

analysieren und die Ergebnisse solcher Analysen nur im Rahmen der VERTRAGSARBEITEN zu nutzen.

Vorbehaltlich Ziffer 0 wird die TUBAF es ferner unterlassen, INFORMATIONEN nachzuahmen oder zu übernehmen, insbesondere im Wege des sog. „Reverse Engineering", um ARBEITSERGEBNISSE oder Produkte der BASF zurückzuentwickeln, zurückzubauen, zu dekompilieren oder disassemblieren oder, im Falle von Software, zu versuchen, den Quellcode aus dem Objektcode abzuleiten.

Die TUBAF wird INFORMATIONEN bzw. damit hergestellten Materialien jederzeit auf Wunsch der BASF entweder sofort an BASF vollständig zurückgeben oder unverzüglich vollständig zerstören bzw. elektronisch übermittelte und/oder gespeicherte Informationen und technische Kenntnisse vollständig löschen.

Vereinbarung

zwischen

Herr Prof. Dr. Urs A. Peuker
- nachfolgend Themengeber genannt -

und dem/der Studierenden Sainzaya Odbayar
.....
- nachfolgend Themennehmer genannt -

zur ausgegebenen ~~Studien-/ Projekt-/Diplom-/ Magister-/~~ Bachelor-/ ~~Masterarbeit~~[1] - nachfolgend Arbeit genannt –

Titel:

Validation of an alternative analyzation method for manual sorting to analyze larger particle size fractions from the re-cycling of lithium-ion batteries (LIB)

Präambel:

Dem Themennehmer ist bekannt, dass die Ergebnisse seiner Arbeit in ein Drittmittel-Forschungsprojekt der Hochschule einfließen und die TU Bergakademie Freiberg im Rahmen dieses Drittmittel-Forschungsprojektes an die im zugehörigen FuE-Vertrag bzw. in zugehörigen Förderbedingungen getroffenen Festlegungen gebunden ist.

Es entspricht dem Wunsch des Themennehmers, dass er vom Themengeber die o.g. Arbeit zur Bearbeitung erhält. Für diese Arbeit gelten die nachfolgenden Bedingungen. Der Themennehmer wurde darauf hingewiesen, dass er auch ein anderes Thema hätte erhalten können, für das diese Bedingungen nicht gelten.

Folgende Vereinbarungen werden getroffen:

1.
Der Themennehmer räumt dem Themengeber und - sofern im FuE-Vertrag/in den Förderbedingungen so festgelegt[1] – auch dem Drittmittelgeber das ausschließliche Nutzungsrecht zur Vervielfältigung und Verbreitung der Arbeit insgesamt oder in Teilen oder ihrer wesentlichen Ergebnisse als Schriftwerk ein. Der Themengeber bzw. der Drittmittelgeber ist jedoch zu einer Vervielfältigung und Verbreitung nicht verpflichtet.

Bei einer Vervielfältigung oder Verbreitung ist der Name des Themennehmers neben dem des betreuenden Hochschullehrers aufzuführen; in geeigneter Weise ist auf die Arbeit als Grundlage der Veröffentlichung hinzuweisen.

2.
Der Themennehmer überträgt dem Themengeber sämtliche ihm zustehenden Rechte an seiner Arbeit zur Verwertung an und durch die TU Bergakademie Freiberg selbst bzw. durch den Drittmittelgeber.

Bezüglich schutzrechtsfähiger Erfindungen gelten folgende Modalitäten:

[1] Nichtzutreffendes streichen

2.1.
Der Themengeber ist zunächst verpflichtet und allein berechtigt, eine aus der Arbeit resultierende schutzrechtsfähige Erfindung zur Erteilung eines Schutzrechts anzumelden. Die Anmeldung hat unverzüglich zu geschehen.

Die Verpflichtung des Themengebers zur Anmeldung entfällt, wenn
- der Themennehmer der Nichtanmeldung zustimmt,
- berechtigte Belange es erfordern, die patentfähige Erfindung nicht bekannt werden zu lassen,
- der Themengeber unverzüglich schriftlich erklärt, dass er der Verpflichtung zur Anmeldung nicht nachkommen wird und deshalb der Themennehmer berechtigt ist, die Erfindung selbst anzumelden.

Der Themengeber ist berechtigt, die Erfindung auch im Ausland anzumelden. Er wird dem Themennehmer mitteilen, in welchen Ländern eine Schutzrechtsanmeldung erfolgen soll.
Der Themennehmer wird den Themengeber auf Verlangen beim Erwerb von Schutzrechten unterstützen und die erforderlichen Erklärungen abgeben.

2.2.
Der Themengeber ist berechtigt, im Rahmen des Drittmittel-Forschungsprojektes oder im Zuge einer wirtschaftlichen Verwertung durch die TU Bergakademie Freiberg schutzrechtsfähige Erfindungen, Schutzrechtsanmeldungen oder Schutzrechte auf einen Dritten zu übertragen.
Der Themengeber wird in einem solchen Fall die Regelungen zur Rechtsübertragung so gestalten, dass die Zahlung einer Erfindervergütung für den Themennehmer abgesichert ist.

2.3.
Will der Themengeber bzw. der Dritte die Schutzrechtsanmeldung nicht weiter verfolgen oder das erteilte Schutzrecht nicht aufrechterhalten, wird er dies dem Themennehmer mitteilen und ihm auf dessen Verlangen das Recht übertragen und die zur Wahrung des Rechts erforderlichen Unterlagen aushändigen.
Der Themengeber bzw. der Dritte ist berechtigt, das Recht aufzugeben, sofern der Themennehmer nicht innerhalb von 2 Monaten nach Zugang der Mitteilung die Übertragung des Rechts verlangt.

3.
Dem Themennehmer ist bekannt, dass er wegen des Praxisbezuges seiner Arbeit an der Hochschule und erforderlichenfalls auch beim Drittmittelgeber Informationen erhalten und Einblick in Unterlagen nehmen wird, die er vertraulich zu behandeln hat und Dritten nicht zugänglich machen darf.

Dem Themennehmer ist weiterhin bekannt, dass er ggf. Hard- und Software benutzen wird, für deren ordnungsgemäße Verwendung und Überwachung der Themen- oder Drittmittelgeber entsprechend abgeschlossener Lizenzverträge und Abmachungen verantwortlich ist.
Der Themennehmer verpflichtet sich insoweit zur absoluten Vertraulichkeit und größtmöglichen Sorgfalt. Dem Themennehmer ist bekannt, dass eine Nichtbeachtung der Festlegungen zur Vertraulichkeit und zur Behandlung geschützter Hard- und Software zu strafrechtlichen oder zivilrechtlichen Schritten führen kann (insbesondere Schadensersatzforderungen).

Freiberg, ...
Themengeber

Freiberg, 17.11.2025
D. Baumgarten
Themennehmer

Appendix B: User manual

Before starting any work with battery recyclables, ensure appropriate personal protective equipment (PPE) is worn at all times. BM dust is hazardous — at minimum, wear gloves, safety glasses, and a dust mask or respirator rated for fine particulate matter. Work in a well-ventilated area or under a fume hood where possible.

1. Place the foil fraction into a separate bucket with a width similar to the ShredCat feed opening (220 mm). This ensures uniform material flow during feeding. Fill the bucket to approximately 80% capacity — overfilling makes controlled feeding difficult.
2. Before feeding, check for metal casings in the foil fraction. These are typically pressed into irregular and bulky shapes that may exceed the width of the feed opening. If a metal casing can be flattened by hand safely, flatten it before feeding. If it cannot be handled safely or flattened, do not force it into the ShredCat — set it aside.
3. Feed the material slowly and at a controlled pace. The foil fraction contains separator foils that are large but very light. Applying too much downward force during feeding can cause them to jump out of the feed opening. Let the material feed gradually rather than pushing it down.
4. Operate the ShredCat in 10-minute intervals with a 10-minute rest period between each pass. The machine heats up after approximately 4 consecutive work sessions. Continuing operation without rest periods risks motor failure — the first ShredCat unit used in this study broke down due to continuous use without breaks. Always allow the machine to cool before resuming if it feels warm to the touch.
5. After the first crushing pass, collect all output material and feed it into the ShredCat again for the second pass using the same procedure as steps 1 to 4.
6. During rotary splitting, uniform and controlled feed flow is critical for representative sub-sampling. Pour the material at a slow and steady speed — pouring too fast causes uneven distribution across the chutes and introduces sub-sampling error. Do not dump the material in one motion.

Appendix C: Raw data

Table 12. Raw data for model material

№	Al2373	Co2286	Cu2247	Fe2332	Li6707	Mn2949	Ni2165	P1782
	wt.-%	wt.-%	wt.-%	wt.-%	wt.-%	wt.-%	wt.-%	wt.-%
BM	0.35	4.34	0.87	0.03	3.91	1.57	29.05	0.45
BA04	12.39	1.34	11.23	0.20	1.29	0.57	9.18	0.14
BA05	22.54	2.08	22.30	0.32	1.84	0.91	14.48	0.20
BA06	11.04	1.47	12.80	0.22	1.43	0.62	10.15	0.15
BA07	22.29	2.09	22.51	0.28	1.83	0.93	14.70	0.21
BA08	13.23	1.39	13.63	0.22	1.36	0.60	9.69	0.14
BA09	24.00	2.06	22.68	0.30	1.79	0.92	14.39	0.22
BA10	11.87	1.47	12.02	0.18	1.32	0.60	9.82	0.15
BA20	22.22	2.09	23.41	0.30	1.82	0.81	13.07	0.16
BA21	22.37	2.16	22.30	0.46	1.93	0.87	13.95	0.18

Table 13. Raw data for manual sorting vs ShredCat analysis

№	Al	Co	Cu	Fe	Li	Mn	Ni	P
	wt.-%	wt.-%	wt.-%	wt.-%	wt.-%	wt.-%	wt.-%	wt.-%
1	7.06	3.13	0.12	0.07	1.54	2.70	4.19	1.35
2	6.87	3.27	0.11	0.07	1.48	2.73	3.72	1.48
3	6.68	3.35	0.14	0.08	1.46	2.73	3.67	1.59
4	13.82	1.89	0.88	0.11	0.96	1.47	2.02	1.69
5	4.05	6.56	19.18	0.06	2.51	6.04	6.54	0.81
6	9.93	1.59	0.40	0.04	1.44	0.34	8.09	1.67

Table 14. Raw data for real foil fraction with different cell types

№	Al	Co	Cu	Fe	Li	Mn	Ni	P
	wt.-%	wt.-%	wt.-%	wt.-%	wt.-%	wt.-%	wt.-%	wt.-%
1	17.67	1.06	28.46	0.11	1.61	0.16	11.94	0.39
2	21.96	1.64	22.28	0.45	1.50	0.53	10.03	0.42
3	23.92	1.62	21.67	0.14	1.57	0.03	11.69	0.48